

Original Article



OPEN ACCESS

Received: Jun 11, 2025

Revised: Aug 19, 2025

Accepted: Sep 17, 2025

Published online: Oct 14, 2025

*Correspondence to

Youn Wook Chung

Department of Biomedical Sciences, Yonsei University College of Medicine, 50-1 Yonsei-ro, Seodaemun-gu, Seoul 03722, Korea.
Email: chungyw@yuhs.ac

Ji-Hwan Ryu

Department of Biomedical Sciences, Yonsei University College of Medicine, 50-1 Yonsei-ro, Seodaemun-gu, Seoul 03722, Korea.
Email: yjh@yuhs.ac

*Kyeongeun Kwon, Minyoung Kim, and Youngrak Jung contributed equally to this work.

Copyright © 2025. The Korean Association of Immunologists

This is an Open Access article distributed under the terms of the Creative Commons Attribution Non-Commercial License (<https://creativecommons.org/licenses/by-nc/4.0/>) which permits unrestricted non-commercial use, distribution, and reproduction in any medium, provided the original work is properly cited.

ORCID iDs

Kyeongeun Kwon

<https://orcid.org/0009-0001-8130-3825>

Minyoung Kim

<https://orcid.org/0009-0008-2585-1457>

Youngrak Jung

<https://orcid.org/0000-0001-7893-1866>

Mi Young Yoon

<https://orcid.org/0000-0001-9309-2204>

Intestinal Dysbiosis Caused by Epithelial *Fabp6* Gene Disruption Exacerbates Gut Inflammatory Disease

Kyeongeun Kwon ^{1,2,†}, Minyoung Kim ^{3,†}, Youngrak Jung ^{4,†},
Mi Young Yoon ⁴, June-Yong Lee ⁴, Sang Sun Yoon ⁴, Mina Rho ^{3,5},
Youn Wook Chung ^{1,*}, Ji-Hwan Ryu ^{1,2,*}

¹Department of Biomedical Sciences, Yonsei University College of Medicine, Seoul 03722, Korea

²Brain Korea 21 Project, Yonsei University College of Medicine, Seoul 03722, Korea

³Department of Artificial Intelligence, Hanyang University, Seoul 04763, Korea

⁴Department of Microbiology and Immunology, Yonsei University College of Medicine, Seoul 03722, Korea

⁵Department of Computer Science, Hanyang University, Seoul 04763, Korea






ABSTRACT

Ileal lipid binding protein (Ilbp), encoded by *Fabp6* gene, plays a critical role in intracellular transport of bile acids (BAs) from apical to basolateral side of ileal enterocytes, maintaining BA homeostasis within enterohepatic circulation. However, pathophysiological consequences of Ilbp deficiency remain largely unexplored. Here, we demonstrate that disruption of BA balance, caused by intestinal epithelial cell (IEC)-specific *Fabp6* gene knockout (*Fabp6*^{ΔIEC}), exacerbates dextran sulfate sodium (DSS)-induced gut inflammation. Fecal microbiota transplantation from *Fabp6*^{ΔIEC} mice to germ free recipient mice replicated the adverse effects observed in *Fabp6*^{ΔIEC} mice, which were mitigated when these mice were co-housed with control (*Fabp6*^{fl/fl}) mice. Metagenomic analysis identified *Ligilactobacillus murinus* as a primarily diminished strain in *Fabp6*^{ΔIEC} mice. Oral administration of *L. murinus* isolated from feces of *Fabp6*^{fl/fl} mice ameliorated DSS-induced colitis in *Fabp6*^{ΔIEC} mice by restoring epithelial barrier integrity and lowering pro-inflammatory cytokines IL-1β, IL-6 and TNF-α. Furthermore, daily administration of taurodeoxycholic acid—one of the BAs reduced in *Fabp6*^{ΔIEC} mice and that promotes the growth of *L. murinus* in an *in vitro* growth assay—also exhibited a protective effect against DSS-induced colitis through a similar mechanism. These findings suggest that deficiency of specific BAs due to epithelial *Fabp6* deletion leads to gut dysbiosis, predisposing the host to inflammatory disease.

Keywords: Fatty acid-binding protein 6; Inflammatory bowel diseases; Microbiome; Bile acid; Colitis

INTRODUCTION

Bile acids (BAs) are synthesized from cholesterol in the liver and secreted by hepatocytes into the intestinal lumen. In the intestine, BAs function as detergents, facilitating the digestion and absorption of fats and fat-soluble vitamins (1). More than 90% of BAs are reabsorbed in the ileum and transported back to the liver through the portal vein (2). This enterohepatic

June-Yong Lee 
<https://orcid.org/0000-0002-4476-725X>
 Sang Sun Yoon 
<https://orcid.org/0000-0003-2979-365X>
 Mina Rho 
<https://orcid.org/0000-0002-2724-9477>
 Youn Wook Chung 
<https://orcid.org/0000-0002-4382-1410>
 Ji-Hwan Ryu 
<https://orcid.org/0000-0001-6969-7465>

Conflict of Interest

The authors declare no potential conflicts of interest.

Abbreviations

ANI, average nucleotide identity; Asbt, apical sodium-dependent bile acid transporter; BAs, bile acids; CA, cholic acid; CD, Crohn's disease; CDCA, chenodeoxycholic acid; CFU, colony-forming unit; cKO, conditional knockout; Cyp7a1, Cholesterol 7 α -hydroxylase; DAI, disease activity index; DCA, deoxycholic acid; DSS, dextran sulfate sodium; Fgf15, fibroblast growth factor-15; FMT, fecal microbiota transplantation; Fxr, farnesoid X receptor; GCA, glycocholic acid; GF, germ-free; HMP, Human Microbiome Project; IBD, inflammatory bowel disease; IEC, intestinal epithelial cell; IHC, immunohistochemistry; Ilbp, ileal lipid binding protein; KEGG, Kyoto Encyclopedia of Genes and Genomes; KO, knockout; LCA, lithocholic acid; MRS, de Man–Rogosa–Sharpe; Ost α -Ost β , organic solute transporter α - β ; PCoA, principal coordinates analysis; qPCR, quantitative PCR; RPKM, reads per kilobase of transcript per million mapped reads; RT-qPCR, real-time quantitative PCR; SPF, specific pathogen free; TCA, taurocholic acid; TDCA, taurodeoxycholic acid; TTBS, Tris-buffered saline containing 0.5% Tween 20; T β -MCA, Tauro- β -muricholic acid; UC, ulcerative colitis; UDCA, ursodeoxycholic acid; WT, wild-type; β -MCA, β -muricholic acid.

Author Contributions

Conceptualization: Kwon K, Chung YW, Ryu JH; Data curation: Kwon K, Kim M, Rho M, Chung YW; Formal analysis: Kim M, Rho M; Funding acquisition: Chung YW, Ryu JH; Methodology: Jung Y, Yoon MY, Lee JY, Yoon SS; Project administration: Chung YW, Ryu JH; Resources: Jung Y, Yoon MY, Lee JY, Yoon SS; Software: Kim M, Rho M; Supervision: Chung YW, Ryu JH; Validation: Jung Y, Lee JY; Visualization: Kwon K, Chung YW; Writing - original draft: Kwon K, Chung YW; Writing - review & editing: Ryu JH.

circulation of BAs is crucial for maintaining their pool size and concentration while limiting their distribution, as these molecules can act as cytotoxic detergents (3).

The major transporters involved in the enterohepatic circulation of BAs have been identified. In the distal ileum, BAs are taken up into the enterocyte by the apical sodium-dependent bile acid transporter (Asbt or ibat; *Slc10a2*) (4), bind to the cytosolic ileal lipid binding protein (Ilbp or Ibapp; *Fabp6*) for intracellular shuttling (5), and are then exported across the basolateral membrane by the heteromeric organic solute transporter α - β (Ost α -Ost β ; *Slc51a-Slc51b*) (6). Changes in the expression of these transporters can regulate intracellular BA levels and, consequently, influence the farnesoid X receptor (Fxr)-mediated regulation of fibroblast growth factor-15 (Fgf15) production, a critical regulator of the negative feedback suppression of BA synthesis (7). Asbt-null mice exhibit a typical BA malabsorption phenotype, characterized by increased fecal BA excretion and a reduced BA pool size, the total BA content of the small intestine, liver, and gallbladder. These changes are accompanied by upregulation of cholesterol 7 α -hydroxylase (Cyp7a1), the rate-controlling enzyme of the classical BA biosynthetic pathway, which enhances hepatic BA synthesis (8). In contrast, Ost α -null mice show no significant changes in fecal BA excretion; however, the BA pool size is reduced to nearly the same extent as in Asbt-null mice (9). Ilbp-null mice (*Fabp6* knockout [KO]), on the other hand, exhibit a trend toward increased fecal BA excretion and reduced BA pool size, along with decreased expression of *Cyp7a1* and *Ost β* (10). In particular, *Fabp6* KO mice are known to exhibit altered energy metabolism influenced by dietary components, a phenomenon attributed to changes in gut microbiota composition (11). However, the direct relationship between host *Fabp6* and the gut microbiota remains poorly understood. Classification and metabolic relationships of BAs are important because BAs exist in multiple forms and their composition is regulated by complex mechanisms, including hepatic synthesis and conjugation, as well as microbiota-mediated modifications in the intestine. Each class of BA—primary, conjugated, and secondary—has distinct origins, physiological functions, and implications for host metabolism and inflammation (**Supplementary Table 1**). Given that *Fabp6* plays a critical role in the reabsorption of BAs from the intestine to the liver, its disruption may impair BA homeostasis. Therefore, class-specific quantification of BAs provides important insight into how *Fabp6* deficiency alters enterohepatic circulation and microbiota-derived BA metabolism.

The gut microbiota, the body's largest reservoir of microbes, performs various essential functions for the host, including digesting substrates inaccessible to host enzymes, suppressing harmful microorganisms, and educating the immune system (12). A diverse array of microbial species resides in the gastrointestinal tract, but dysbiosis—an imbalance in the gut microbiota—can lead to a wide range of diseases, from localized gastrointestinal disorders to metabolic, hepatic, neurologic, respiratory, and cardiovascular illnesses (13,14). Maintaining a balanced composition of gut microbiota is crucial for preserving normal mucosal physiology, as disruptions can contribute to the pathophysiology of many gastrointestinal disorders, including inflammatory bowel disease (IBD). IBD, which includes Crohn's disease (CD) and ulcerative colitis (UC), is a group of progressive inflammatory disorders affecting an estimated 6.8 million people worldwide, with an increasing incidence and need for effective treatments (15). The pathogenesis of IBD is thought to result from dysregulation of the mucosal immune system, which triggers a pathogenic inflammatory response against the commensal gut flora. The proportions of bacterial phyla, particularly Bacteroidetes and Firmicutes, differ significantly from those in non-IBD controls, with a reduced abundance of Bacillus (predominantly *Lactobacillus*) in IBD patients (16). Immune

cells in the intestinal mucosa secrete cytokines in response to microbial products or Ags from the commensal microbiota, playing a critical role in the pathogenesis of severe and progressive forms of IBD (17). Some species of *Lactobacillus* have been shown to suppress experimentally induced colitis by inducing IL-10 production (18,19). The intestinal mucosa exists in a functional equilibrium with the complex luminal environment, dominated by a spectrum of microbial species and their products. Many IBD susceptibility loci suggest an impaired response to microbes in the disease, though the causality of this relationship remains unclear (20-22).

In this study, we generated intestinal epithelial cell (IEC)-specific *Fabp6* KO (*Fabp6*^{ΔIEC}) mice to investigate BA-microbiome interactions in gut inflammation using a dextran sulfate sodium (DSS)-induced colitis model. We conducted targeted metabolomic analyses and metagenomic sequencing of cecal contents to identify specific metabolites and bacteria that influence colitis severity (materials and methods of the study in **Supplementary Data 1**). Our findings reveal that *Fabp6* deletion in the intestinal epithelium reduces specific BA species, particularly taurocholic acid (TCA), chenodeoxycholic acid (CDCA), and taurodeoxycholic acid (TDCA). This altered gut environment diminished the abundance of *Ligilactobacillus murinus* (previously known as *Lactobacillus murinus*) and decreases the Firmicutes/Bacteroidetes ratio, a shift associated with increased susceptibility to gut inflammation. DSS-induced colitis severity in *Fabp6*^{ΔIEC} mice was alleviated by oral administration of *L. murinus* or TDCA, improving intestinal barrier integrity and normalizing pro-inflammatory cytokine levels. These results highlight a BA-intestinal microbiome-gut inflammation axis and propose *L. murinus* and TDCA as potential probiotic and prebiotic candidates to mitigate gut inflammatory diseases.

MATERIALS AND METHODS

Mice

Fabp6 floxed (*Fabp6*^{fl}) mice were generated by Korean Mouse Phenotyping Center (KMPC; *Fabp6*^{em1(KMPC)/YJL}). Villin1-Cre mice were obtained from the Jackson Laboratory (stock number 021504; Bar Harbor, ME, USA) and used to inactivate genes in villus and crypt epithelial cells of small and large intestine. To generate intestine epithelial cells specific conditional knockout *Fabp6* mouse (*Fabp6*^{ΔIEC}), *Fabp6*^{fl} mice were crossed with Villin1-Cre mice. *Fabp6*^{ΔIEC} and *Fabp6*^{fl} mice were separately maintained and bred under specific pathogen free conditions. For co-housing experiment, *Fabp6*^{fl} and *Fabp6*^{ΔIEC} littermates were housed together. Germ-free (GF) mice (C57BL/6) were bred and housed in flexible-film isolators (Class Biologically Clean Ltd., Madison, WI) in the gnotobiotic animal facility of Yonsei University College of Medicine. GF mice were provided sterile water and fed autoclaved chow diet ad libitum. GF status was monitored regularly by aerobic and anaerobic culturing of mouse feces. For fecal microbiota transplantation (FMT) experiment, GF mice were transferred to isocages (Tecniplast Inc., West Chester, PA, USA) for each experimental group. All experiments in this study were conducted exclusively on male mice. All animal work was approved by the Institutional Animal Care and Use Committee at Yonsei University College of Medicine (protocol number 2018-0234 and 2023-0207), according to guidelines outlined by the Association for Assessment and Accreditation of Laboratory Animal Care International (facility number 001071). The genotypes of mice were determined by PCR amplification of tail DNA using the following primers: *Fabp6*-5-F: AAG GAA GGA AGA ACA GTT CCA GTT; *Fabp6*-3-R: AGT GTA GTA GCA GCC ATT TGT ATC.

Real-time quantitative PCR (RT-qPCR)

RT-qPCR was performed on samples from the ileum and liver. Total RNA for tissues was extracted by Hybrid-R™ (305-101; GeneAll Biotechnology, Seoul, Korea). RNA was quantified by NANODROP 100 spectrophotometer (Thermo Fisher Scientific, Waltham, MA, USA), and cDNA was reverse transcribed using PrimeScript™ RT Master Mix (RR036A; TaKaRa, Shiga, Japan) according to the manufacturer's instruction. For RT-qPCR, KAPA SYBR FAST quantitative PCR (qPCR) master mix (2×) was used according to the manufacturer's instruction. qPCR reaction was performed using QuantStudio 3 Real-Time PCR using KAPA SYBR® FAST ABI Prism® (Thermo Fisher Scientific). The gene expression levels were evaluated using the comparative Ct method ($2^{-\Delta\Delta C_t}$ method). The primer sequences were listed in **Supplementary Table 2**.

Western blot analysis

Mouse ileum tissues were lysed in radioimmunoprecipitation assay buffer containing the Halt™ Protease & Phosphatase Inhibitor Single-Use Cocktail, EDTA-free (100×). Total protein concentration was quantified using the Pierce™ BCA Protein Assay Kit according to the manufacturer's instructions (#23225; Thermo Fisher Scientific). Protein samples (20 µg) at equal concentrations were loaded onto 10% SDS-PAGE gels, and the proteins were transferred to polyvinylidene fluoride membranes (Merck Millipore, Burlington, MA, USA). Membranes were blocked for 1 h at room temperature in 5% skim milk in Tris-buffered saline (50 mM Tris-Cl, pH 7.5, 150 mM NaCl) containing 0.5% Tween 20 (TTBS). They were then incubated overnight at 4°C with primary Abs (1:1,000 dilution) in 5% skim milk. After three washes with TTBS, membranes were incubated with secondary Abs (1:3,000 dilution) in 5% skim milk for 1 h. Bands were visualized using Pierce ECL Western Blotting Substrate (Thermo Fisher Scientific) and detected on X-ray film. The primary Abs used were rabbit anti-FABP6 (orb412509; Biorbyt, Cambridge, UK) and mouse anti-GAPDH (sc-32233; Santa Cruz Biotechnology, Dallas, TX, USA).

Immunohistochemistry (IHC)

For IHC staining, formalin-fixed paraffin-embedded small intestine and colon sections from *Fabp6^{flf}* and *Fabp6^{ΔIEC}* mice were stained with FABP6 Ab (orb412509; Biorbyt) and counterstained with H&E. IHC analysis was performed as previously described (23). Primary Abs (1:500) were applied overnight at 4°C. Staining was visualized using an Olympus BX43 microscope with the Olympus CellSens Entry software (Olympus, Tokyo, Japan).

Bile acid extraction and quantification by mass spectrometry

The cecal contents of mice were collected and weighed. To minimize variations in BA levels due to circadian rhythm, all cecal samples were collected at approximately the same time (between 9:00 and 10:00 AM). Approximately 50 mg of the cecal contents was dissolved in methanol for metabolite extraction. The column was pre-washed with methanol before loading the solution onto it. The mixture was then centrifuged and filtered (9,100 ×g, 4°C, 60 min), and the supernatant was collected for subsequent analysis using Rapid LC/MS/MS Spectrometer (Thermo Fisher Scientific). Nine bile acids were used as standard for this analysis: TCA (86339; Sigma, St. Louis, MO, USA), glycocholic acid (GCA, G7132; Sigma), Tauro-β-muricholic acid (Tβ-MCA, #20289; Cayman, Grand Cayman, Cayman Islands), cholic acid (CA, C1129; Sigma), CDCA (C9377; Sigma), β-muricholic acid (β-MCA, SML2372; Sigma), ursodeoxycholic acid (UDCA, U5127; Sigma), deoxycholic acid (DCA, D6750; Sigma), lithocholic acid (LCA, L6250; Sigma), and TDCA (SC-281164; Santa Cruz Biotechnology). A calibration curve was generated using these standards for quantification.

DSS-induced colitis mouse model

At 8–9 wk of age, mice were treated with 2.5% (w/v) DSS (molecular weight: 36,000–5,000; MP Biomedicals, Irvine, CA, USA) dissolved in drinking water for 5 or 7 days, replaced with normal drinking water for following experimental days. Mice were monitored daily for changes in weight and disease activity index (DAI). Weight loss was scored as follows: 0, none; 1, 1%–5%; 2, 5%–10%; and 4, >20%. Stool consistency was scored as follows: 0, normal; 2, loose stool; 4, diarrhea. The bleeding score was assigned as follows: 0, no blood in stool; 1, light and faint; 2, clear and visible; 4, gross rectal bleeding. On day 9, mice were euthanized, and the colon were harvested and colon length was measured. The survival of the mice was monitored for 14 days.

Histologic analysis

Colon tissues were dissected and immediately fixed with 4% paraformaldehyde for histologic analyses. Paraffin-embedded sections of colonic tissues were stained with H&E. Colonic injury was assessed using histological scoring system. Briefly, the histological score was the sum of the scores for inflammatory cell infiltration (0, normal; 1, mucosa; 2, mucosal and submucosa; 3, transmural), crypt damage (0, none; 1, basal 1/3 damage; 2, basal 2/3 damaged; 3, only epithelium intact; 4, crypt and surface epithelium lost) and percentage involvement (0, 0%; 1, 1%–25%; 2, 26%–50%; 3, >51%) (24).

FMT

For FMT experiment, GF mice at 4–5 wk of age transfer to isocages. Fecal samples of donor mice (100 mg) were suspended in 1 ml of sterile PBS and homogenized. After centrifugation at 100 ×g for 1 min, the supernatant was used to gavage recipient mice (200 µl per mouse). After colonization, mice were rested for 3 weeks prior to treatment, during which cages were only changed if necessary.

Shotgun sequencing of the metagenome

Sequencing libraries were prepared using the TruSeq Nano DNA High Throughput Library Prep Kit (Illumina, San Diego, CA, USA) according to the manufacturer's instructions. Briefly, 100 ng of genomic DNA was fragmented using Covaris' adaptive focused acoustic technology. The fragmented DNA was end-repaired to produce 5'-phosphorylated, blunt-ended dsDNA molecules. After end-repair, DNA fragments were size-selected through a bead-based method. A single 'A' base was then added, followed by ligation of the TruSeq DNA UD Indexing adapters. The library products were purified and amplified by PCR to create the final library. Library quantification was performed by qPCR using the KAPA Library Quantification Kit (for Illumina Sequencing) according to the qPCR Quantification Protocol Guide and accessed on the Agilent Technologies 4200 TapeStation D1000 ScreenTape (Agilent Technologies, Santa Clara, CA, USA). Sequencing was conducted on the HiSeq 4000 platform (Illumina).

Metagenome data analysis

The relative abundance of taxa was calculated for each sample using Kraken v2.1.3 (25) for taxonomic classification and Bracken v2.9 (26) for abundance estimation refinement with default parameter settings. This combined approach ensures a robust and precise determination of the taxonomic composition and abundance in metagenomic datasets.

To visualize the taxonomic composition, alpha-diversity and beta-diversity analyses were conducted. Alpha-diversity measures the diversity within a single sample. The metrics

for calculating alpha-diversity include richness, Shannon's diversity, Simpson's diversity, Simpson's dominance estimator (27). To quantify beta-diversity, principal coordinates analysis (PCoA) was conducted using Bray-Curtis dissimilarity as a distance metric. By projecting the samples into a 2-dimensional space, PCoA highlights clusters of samples with similar taxonomic compositions and reveals gradients of variation between them.

For functional analysis, we measured the relative abundance of pathway categories based on Kyoto Encyclopedia of Genes and Genomes (KEGG) databases (28). For read alignment, we used the DIAMOND (29) with 40% sequence identity cutoff and 40% query coverage cutoff. Based on the alignment results from DIAMOND, we calculated the reads per kilobase of transcript per million mapped reads (RPKM) for each gene to quantify its relative abundance.

Considering KEGG annotation, each gene was mapped to a corresponding K number. To determine the RPKM for each K number, the RPKM values of all genes associated with a specific K number were summed. Subsequently, we filtered the K numbers with a log2 fold change of 2 or higher and these filtered K numbers were then subjected to pathway mapping using KEGG database to determine which pathways showed significant differences between the two groups.

Bacterial isolation and identification

A *L. murinus* strain was isolated from *Fabp6^{flf}* mice and identified through 16S rRNA sequencing. For bacterial isolation, feces from *Fabp6^{flf}* mice were immediately re-suspended in sterile PBS, homogenized and serially diluted in sterile PBS. The diluted mixture was plated on de Man–Rogosa–Sharpe (MRS) agar plate (MB Cell, Seoul, Korea) and incubated for 16 h at 37°C in a BD™ BBL™ GasPak anaerobic jar (260626; BD Biosciences, San Jose, CA, USA). Grown colonies were re-streaked on fresh MRS agar plates. After incubation, colonies were identified using capillary electrophoresis sequencing by MacroGen (Seoul, Korea). Taxonomic identification was performed by amplifying the 16S rRNA gene using primers 27F (5'-AGA GTT TGA TCM TGG CTC AG-3') and 1492R (5'-TAC GGY TAC CTT GTT ACG ACT T-3'). Verification of the 16S rRNA gene sequence was performed using primers 785F (5'-GGA TTA GAT ACC CTG GTA-3') and 907R (5'-CCG TCA ATT CMT TTR AGT TT-3'). A search of the National Center for Biotechnology Information database revealed that the query sequences matched those derived from *L. murinus*.

L. murinus administration

L. murinus was grown on MRS agar plates at 37°C under anaerobic condition. One colony was picked and used to inoculate 10 ml of MRS medium and cultured for overnight at 37°C. The culture media were centrifuged at 3,000 ×g for 10 min. Pellets were re-suspended in sterile PBS and administered to mice (1×10⁹ colony-forming unit [CFU]/ml) via oral gavage every day, starting 2 days prior to DSS treatment and continuing until the end of the experiment.

Inflammatory cytokine detection by ELISA

Colon tissue samples were collected and washed with PBS. The concentrations of IL-6 (DY406), IL-1β (DY401) and TNF-α (DY410) in the colon tissues were measured using the DuoSet® ELISA kit (R&D Systems, Minneapolis, MN, USA) following the manufacturer's instructions. The detection thresholds for IL-6, IL-1β and TNF-α in the ELISA assays were consistently above the pictogram per milliliter (pg/ml) range. Absorbance was measured at 450 nm using the VersaMax™ Microplate Reader (Molecular Devices, San Jose, CA, USA), and the results were analyzed with SoftMax® Pro Software v5.2 (Molecular Devices).

Intestinal permeability

Intestinal permeability was assessed *in vivo* following oral administration of 4 kDa FITC-dextran (46944; Sigma). After food withdrawal (4 h), mice were orally administrated with FITC-dextran (0.6 g/kg body weight). After 4 h, 300 µl of blood was collected in sodium citrate-contained tubes and gently mixed. The tubes were centrifuged at 3,000 ×g for 15 min at 4°C. Collected plasma were diluted with PBS and fluorescence was monitored using microplate reader. Excited at 485 nm and emitted at 528 nm.

Plasma LPS measurement

Blood plasma was collected from the abdominal vein using Greiner Minicollect tubes (450533; Greiner Bio-One GmbH, Kremsmünster, Austria). The samples were centrifuged at 2,000 ×g for 10 min at 4°C, and the separated plasma was stored at -70°C until analysis. Plasma LPS levels were quantified using a LPS ELISA Kit (OKEH02594; Aviva Systems Biology, San Diego, CA, USA) following the manufacturer's instructions.

L. murinus *in vitro* growth assay

From fresh colonies grown on MRS agar plates, a colony was picked and cultured overnight adjusted to OD₆₀₀ of 2.5. For assay, 100 µl of prepared overnight cultures were diluting into a 1.9 ml of the medium containing 10 µM of bile acids. The concentrations were selected to approximate physiological levels found in the gut lumen, based on previously published studies (30,31). The growth of bacteria was monitored every 1 h by OD₆₀₀ measurement using BioTek Cytation™ 5 Cell Imaging Multi-Mode Reader (Agilent Technologies) set at 37°C with 30 s shaking before each time point and use a software (Gen5) for data collection.

L. salivarius *in vitro* growth assay

An *in vitro* growth assay for *L. salivarius* was performed using a 5× Difco™ M9 Minimal medium (#248510; BD Biosciences). To prepare 1 L of 1× M9 minimal medium, the following components were added: 20 ml of filtered 20% glucose (G7528; Sigma) solution, 2 ml of MgSO₄ (M9397; Sigma), 0.1 ml of 1M CaCl₂ (C1016; Sigma), 0.5 mg of thiamine hydrochloride (T4625; Sigma), 5 µl of vitamin K, 1 g of Bacto™ Casamino Acids (#223050; BD Biosciences), 2.5 g of Bacto™ Yeast Extract (#212750; Gibco, Grand Island, NY, USA), and 10 g of MnCl₂ (M3634; Sigma). For the assay, 50 µl of prepared overnight cultures were diluted into 1.95 ml of the M9 medium containing 10 µM of bile acids.

BA administration

TDCA was dissolved in PBS at a concentration of 10 mM. The solution was administered to mice via oral gavage daily throughout the experimental period.

Quantification and statistical analysis

Data were processed and analyzed by GraphPad Prism v10.4.0 software, with results expressed as means ± SEM. For single-variable comparisons, two-tailed unpaired Student's *t*-tests were used. For multi-variable analyses, one-way ANOVA with Tukey's multiple comparisons test or two-way ANOVA with Tukey's multiple comparisons test were applied. A *p*-value <0.05 was considered statistically significant.

Data availability

The accession number for the microbial dataset reported in this study are available at European Nucleotide Archive with the accession number PRJEB81807 (<https://www.ebi.ac.uk/ena>).

RESULTS

IEC-specific *Fabp6* gene deletion causes dysregulation of BA metabolism

To generate mice with selective *Fabp6* deletion in IECs (*Fabp6*^{ΔIEC} mice), we created *Fabp6* floxed mice (*Fabp6*^{fl/fl}) and crossed them with mice constitutively expressing Cre under the Villin promoter (*Villin*^{Cre}). We confirmed the complete loss of *Fabp6* expression (**Fig. 1A**) and its protein product, Ilbp (**Fig. 1B**), in the intestine of *Fabp6*^{ΔIEC} mice. Ilbp was primarily expressed in the distal intestine and was rarely detected in the colon (32), with no expression in the ileum of *Fabp6*^{ΔIEC} mice (**Fig. 1C**). Since Ilbp deficiency tends to reduce the BA pool size (10), we analyzed BA profiles in *Fabp6*^{fl/fl} and *Fabp6*^{ΔIEC} mice using targeted metabolomics. Consistent with previous reports (10,11), Ilbp loss led to substantial alterations in the cecal BA profile due to BA malabsorption. Specifically, levels of TCA (−35.1%), GCA (−50.0%), CA (−90.0%), CDCA (−51.3%), and TDCA (−58.6%) were significantly reduced in *Fabp6*^{ΔIEC} mice compared to *Fabp6*^{fl/fl} mice, while T-βMCA, β-MCA, UDCA, DCA, and LCA remained unchanged (**Fig. 1D**). These findings indicate disrupted BA homeostasis in *Fabp6*^{ΔIEC} mice. However, expression of genes related to BA synthesis (*Cyp7a1*), transport (*Asbt* and *Osta*), homeostasis (*Fxr*, *Shp* and *Fgf15*), and conjugation (*Bacs*) showed no significant differences in the liver (**Supplementary Fig. 1A–E**), ileum (**Supplementary Fig. 2B–F**), or colon (**Supplementary Fig. 2G–K**).

Fabp6 conditional knockout (cKO) mice exhibit exacerbated DSS-induced gut inflammation

To assess whether the dysregulation of BA metabolism caused by the IEC-specific deletion of *Fabp6* affects pathophysiology during DSS-induced colitis, *Fabp6*^{fl/fl} and *Fabp6*^{ΔIEC} mice were separately housed and orally administered 2.5% DSS for 5 days for pathophysiological analysis or 7 days for survival analysis (**Fig. 1E**). After 5 days of DSS treatment, *Fabp6*^{ΔIEC} mice exhibited increased weight loss compared to *Fabp6*^{fl/fl} mice (**Fig. 1F**), accompanied by a higher DAI (**Fig. 1G**), shorter colon length (**Fig. 1H and I**), and an increased histological score (**Fig. 1J and K**). Although the survival rate difference between *Fabp6*^{fl/fl} and *Fabp6*^{ΔIEC} mice was significant but marginal after 5 days of DSS treatment (**Fig. 1L**), we extended the experiment by treating both groups with 2.5% DSS for 7 days and monitoring them daily for changes in body weight and mortality over a 14-day period (**Fig. 1E**). Notably, *Fabp6*^{ΔIEC} mice exhibited significantly worse mortality (73.33%) compared to *Fabp6*^{fl/fl} mice (36.36%) (**Fig. 1M**). These results demonstrate that *Fabp6*^{ΔIEC} mice are more susceptible to DSS-induced colitis than *Fabp6*^{fl/fl} mice. Importantly, even under DSS-induced colitis, the expression of genes associated with BA metabolism showed no significant differences in the gut (**Supplementary Fig. 2**).

We thoroughly investigated the impact of *Fabp6* gene deletion on both innate and adaptive immune responses using the *Helicobacter hepaticus* infection model (**Supplementary Fig. 3A**) (33). Although *H. hepaticus* successfully colonized (**Supplementary Fig. 3B**) and colitis developed following anti-IL-10R Ab treatment in both *Fabp6*^{fl/fl} and *Fabp6*^{ΔIEC} mice, *Fabp6* deletion did not affect T cell differentiation in the mesenteric lymph nodes (**Supplementary Fig. 3C**), nor were any differences observed in the T cell populations within the lamina propria (**Supplementary Fig. 3D**). Furthermore, adoptively transferred Ag-specific T cells showed comparable responses between the two groups (**Supplementary Fig. 3E**). Flow cytometry analysis of immune cell populations in lamina propria lymphocytes isolated from *Fabp6*^{fl/fl} and *Fabp6*^{ΔIEC} mice revealed no significant differences in the numbers of Th1 cells (T-bet⁺ in the Foxp3[−]CD44⁺CD4⁺TCRβ⁺ cells), Tregs (both Rorγt⁺ and Rorγt[−]Foxp3⁺ in the CD44⁺CD4⁺TCRβ⁺ Tregs), or Th17 cells (Rorγt⁺ in the Foxp3[−]CD44⁺CD4⁺TCRβ⁺ Th17 cells)

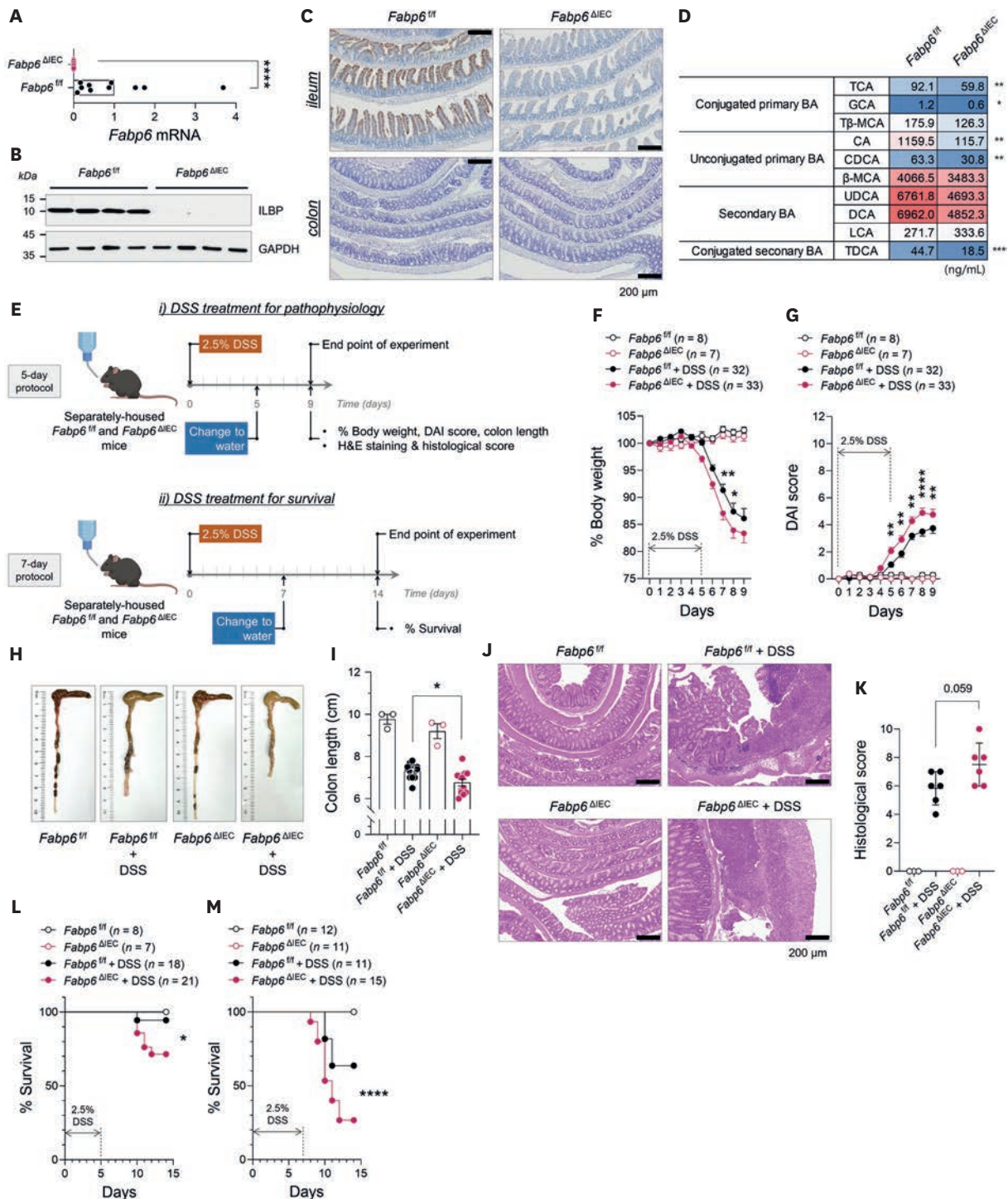


Figure 1. *Fabp6* cKO mice are more susceptible to DSS-induced colitis. (A-C) *Fabp6* expression level in the ileum of *Fabp6^{fl/fl}* and *Fabp6^{ΔIEC}* mice analyzed by qRT-PCR (A), Western blotting (B), and immunohistochemistry (C). (D) Alterations in the cecal bile acid profile of *Fabp6^{fl/fl}* and *Fabp6^{ΔIEC}* mice. (E) Study scheme. Acute colitis was induced in *Fabp6^{fl/fl}* and *Fabp6^{ΔIEC}* mice by administering 2.5% DSS in their drinking water for 5 days (pathophysiology study) or for 7 days (survival experiment). (F) Body weight loss and (G) DAI score were monitored daily for 9 days. Representative images of the colon (H) were taken and colon length (I) was measured on day 9. H&E staining of colon sections (J) and histological scoring (K) of *Fabp6^{fl/fl}* and *Fabp6^{ΔIEC}* mice were performed at the end of the experiment (day 9). Survival rates were monitored daily for 14 days in *Fabp6^{fl/fl}* and *Fabp6^{ΔIEC}* mice with or without DSS-induced colitis. Two different durations of DSS treatment were tested; one group was treated for 5 days (L) and the other for 7 days (M). A mantel cox survival analysis was used to compare the survival rates between groups. Data are presented as mean ± SEM. Statistical significance was determined using two-tailed unpaired Student's *t*-tests (A), two-way ANOVA with Tukey's multiple comparisons test (F, G), or one-way ANOVA with Tukey's multiple comparisons test (I, K).

p*<0.05, *p*<0.01, ****p*<0.001, *****p*<0.0001.

in the ileum (**Supplementary Fig. 4A**), colon (**Supplementary Fig. 4B**), and mesenteric lymph nodes (**Supplementary Fig. 4C**) between *Fabp6^{fl/fl}* and *Fabp6^{ΔIEC}* mice, with comparable cytokine production. Additionally, the numbers of myeloid cells—including dendritic cells, neutrophils, eosinophils, monocytes, and macrophages—were similar in the ileum (**Supplementary Fig. 5A**), colon (**Supplementary Fig. 5B**), and mesenteric lymph nodes (**Supplementary Fig. 5C**) between the two groups. These observations suggest that the increased susceptibility of *Fabp6^{ΔIEC}* mice to gut inflammation is likely due to dysbiosis caused by BA imbalance rather than alterations in immune responses.

Co-housing of *Fabp6* cKO mice with wild-type (WT) mice mitigates DSS-induced colitis

To test whether *Fabp6*-dependent vulnerability to DSS-induced colitis involves commensal microbiota, we co-housed *Fabp6^{ΔIEC}* mice with *Fabp6^{fl/fl}* mice from weaning to adulthood, allowing for microbiota exchange. Following co-housing, the mice were treated with DSS (**Fig. 2A**). Unlike separately housed *Fabp6^{ΔIEC}* mice, those that underwent co-housing showed improved colitis symptoms in response to DSS treatment (**Fig. 2B–G**), suggesting that co-housing allows *Fabp6^{ΔIEC}* mice to acquire a DSS-induced colitis-resistant phenotype, likely through exposure to commensal microbes or related metabolites.

Fecal microbiota transplantation transfers the gut inflammatory phenotype of *Fabp6* cKO mice

To directly assess whether the microbiota of *Fabp6^{ΔIEC}* mice contributes to their susceptibility to DSS-induced colitis, we conducted FMT experiments. Colitis development was analyzed in GF mice following the transfer of gut microbiota from either *Fabp6^{fl/fl}* (GF + *Fabp6^{fl/fl}*-FMT) or *Fabp6^{ΔIEC}* (GF + *Fabp6^{ΔIEC}*-FMT) mice (200 μ l per mouse of 100 mg/ml fecal suspension) (**Fig. 3A**). After DSS treatment, GF + *Fabp6^{ΔIEC}*-FMT mice exhibited more severe colitis compared to GF + *Fabp6^{fl/fl}*-FMT mice, as evidenced by increased weight loss (**Fig. 3B**), higher DAI scores (**Fig. 3C**), shorter colon length (**Fig. 3D and E**), and greater tissue damage in the colon (**Fig. 3F and G**). GF + *Fabp6^{ΔIEC}*-FMT mice also showed higher mortality compared to GF + *Fabp6^{fl/fl}*-FMT mice (**Fig. 3H**). These results confirm that the altered microbiota in *Fabp6^{ΔIEC}* mice is responsible for the increased susceptibility to DSS-induced colitis.

L. murinus is primarily diminished in *Fabp6* cKO mice

To identify differences in microbial composition between *Fabp6^{fl/fl}* and *Fabp6^{ΔIEC}* mice, we analyzed the cecal microbiota using metagenomic sequencing. Bacterial richness and diversity in *Fabp6^{ΔIEC}* mice were assessed through Sobs, Shannon, Simpson, and InvSimpson indices, showing comparable values to *Fabp6^{fl/fl}* mice (**Fig. 4A**). However, PCoA revealed significant compositional differences between the 2 groups, with *Fabp6^{fl/fl}* and *Fabp6^{ΔIEC}* mice clustering separately (**Fig. 4B**). The Firmicutes/Bacteroidetes ratio was substantially lower in *Fabp6^{ΔIEC}* mice than in *Fabp6^{fl/fl}* mice (**Fig. 4C**). Taxonomic profiling indicated shifts in the abundance of key genera (**Fig. 4D**), with *Faecalibaculum rodentium* and *Parabacteroides distasonis* significantly increased in *Fabp6^{ΔIEC}* mice, while *L. murinus* was markedly decreased (**Fig. 4E**). These species were highlighted because the Wilcoxon rank-sum test identified them as significantly different between groups ($p < 0.05$). The reduced abundance of *L. murinus* in *Fabp6^{ΔIEC}* mice was further validated by qPCR (**Fig. 4F**). Pathway analysis suggested an association with pyruvate metabolism, glycolysis/gluconeogenesis, methane metabolism and O-Ag nucleotide sugar biosynthesis (**Supplementary Fig. 6**). For further investigation, we isolated a *L. murinus* strain from *Fabp6^{fl/fl}* feces and conducted a comparative analysis to assess its genetic similarity and phylogenetic placement within the *Ligilactobacillus*

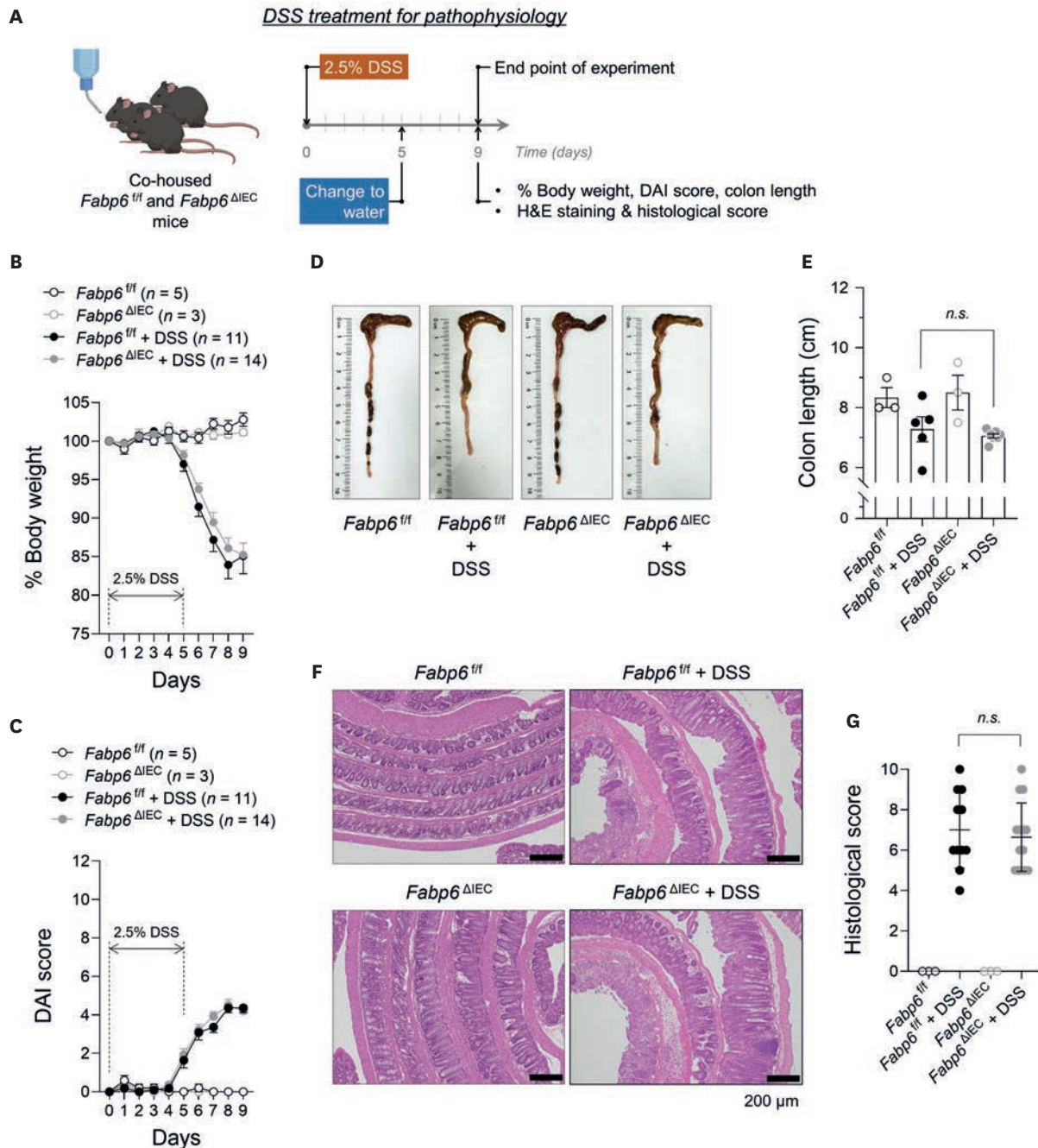


Figure 2. Co-housing of *Fabp6* cKO mice with WT mice mitigates DSS-induced colitis. (A) Study schemes. The co-housed *Fabp6*^{fl/fl} and *Fabp6*^{ΔIEC} mice were treated with 2.5% DSS for 5 days to induce acute colitis. (B) Body weight loss and (C) DAI score were monitored daily for 9 days. Representative images of the colon (D) were taken and colon length (E) was measured on day 9. H&E staining of colon sections (F) and histological scoring (G) of the co-housed *Fabp6*^{fl/fl} and *Fabp6*^{ΔIEC} mice were performed at the end of the experiment (day 9). Data are represented as mean values ± SEM. Significance was determined by two-way ANOVA with Tukey's multiple comparisons test (B, C) or one-way ANOVA with Tukey's multiple comparisons test (E, G). n.s., not significant.

lineage. The new strain referred to as “This study,” showed an average nucleotide identity (ANI) value of 98.1% with *L. murinus* reference strain, and 99.9% similarity with *L. murinus* ASF361 (Fig. 4G). Comparative genomics analysis with dispensable genes further grouped this strain with *L. murinus* ASF361 and YK1 (Supplementary Fig. 7A and B, Supplementary Table 3). A phylogenetic analysis confirmed that our *L. murinus* strain clustered tightly with

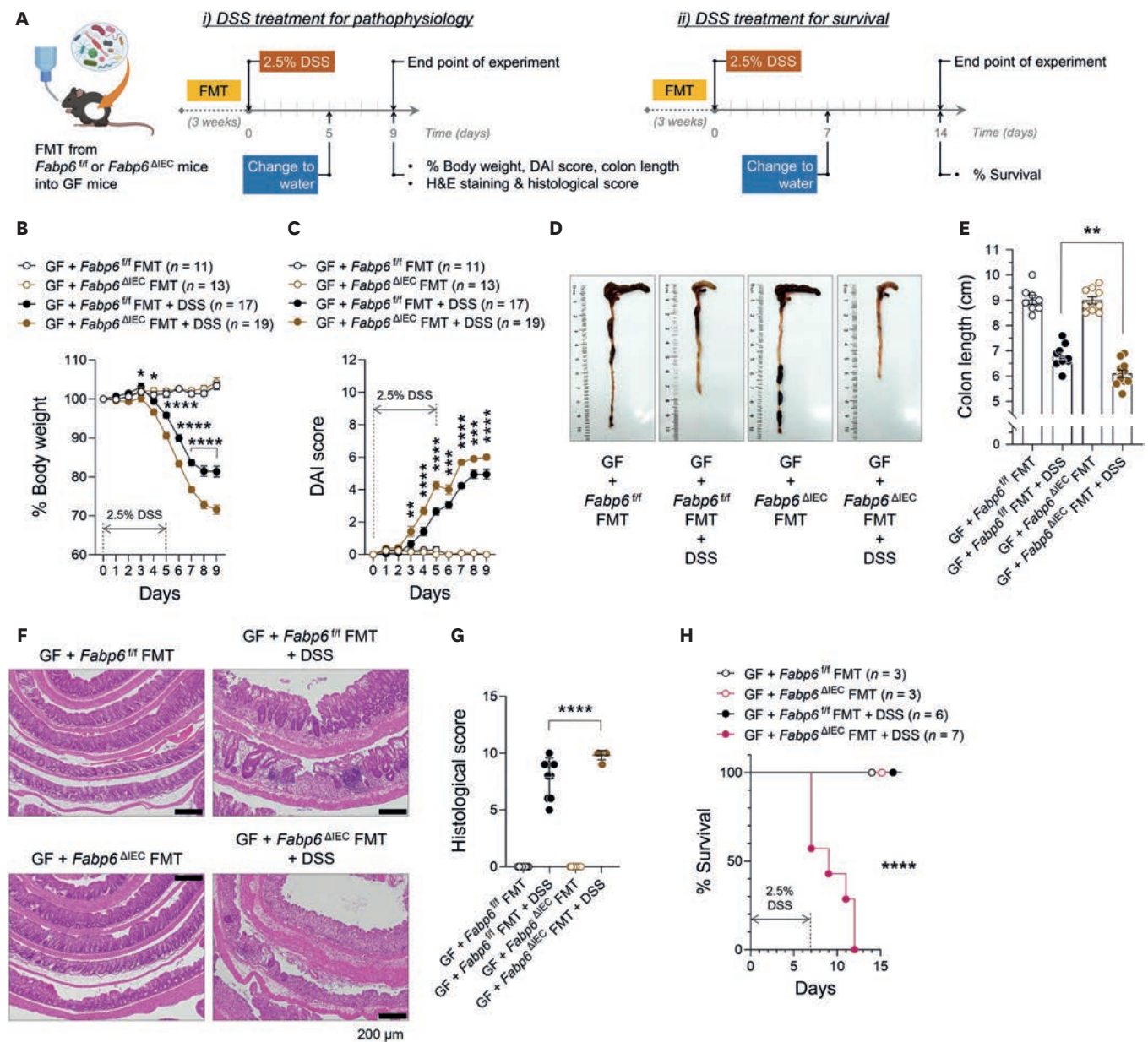


Figure 3. Fecal microbiota transplantation from *Fabp6* cKO exacerbates DSS-induced colitis. (A) Study schemes. GF mice (4–5 wk-old) were transplanted with fecal microbiota from *Fabp6^{fl/fl}* and *Fabp6^{ΔIEC}* mice (200 μl per mouse of 100 mg/ml fecal suspension) and, 3 wk later, treated with 2.5% DSS for 5 or 7 days to induce acute colitis. (B) Body weight loss and (C) DAI score were monitored daily for 9 days. Representative images of the colon (D) were taken and colon length (E) was measured on day 9. H&E staining of colon sections (F) and histological scoring (G) of the recipient *Fabp6^{fl/fl}*-FMT and *Fabp6^{ΔIEC}*-FMT mice were performed at the end of the experiment (day 9). (H) Survival rates were monitored daily for 14 days in the recipient *Fabp6^{fl/fl}*-FMT and *Fabp6^{ΔIEC}*-FMT mice with or without DSS-induced colitis (2.5% for 7 days). A mantel cox survival analysis was used to compare the survival rates between groups. Data are presented as mean ± SEM. Statistical significance was determined using two-way ANOVA with Tukey's multiple comparisons test (B, C) or one-way ANOVA with Tukey's multiple comparisons test (E, G). *p < 0.05, **p < 0.01, ***p < 0.001, ****p < 0.0001.

various *L. murinus* strains, forming a distinct clade (**Supplementary Fig. 7C**). Our observations suggest that the reduced abundance of *L. murinus* in *Fabp6^{ΔIEC}* mice may contribute to their increased susceptibility to DSS-induced colitis.

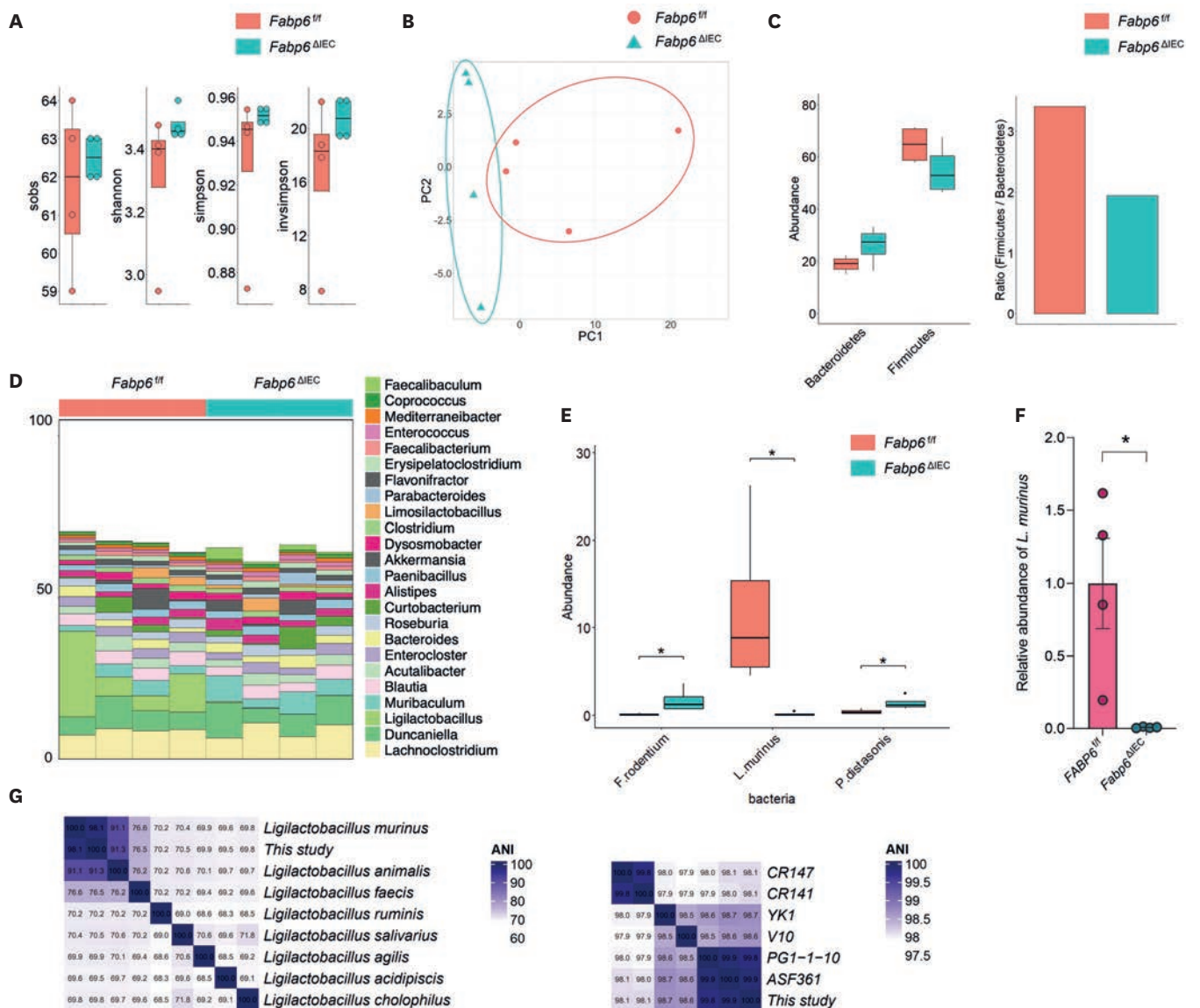


Figure 4. IEC-specific *Fabp6* gene deletion induces dysbiosis of gut microbiota. (A) Estimation of gut bacterial richness and diversity (*Fabp6^{fl/fl}* vs. *Fabp6^{ΔIEC}* mice). (B) PCoA using metagenomics data (*Fabp6^{fl/fl}* vs. *Fabp6^{ΔIEC}* mice) (β -diversity). (C) The abundance of Bacteroidetes and Firmicutes in *Fabp6^{fl/fl}* and *Fabp6^{ΔIEC}* mice (left panel), and the ratio of Firmicutes to Bacteroidetes (right panel). (D) Differential bacterial composition between *Fabp6^{fl/fl}* and *Fabp6^{ΔIEC}* mice at genus level. (E) Relative abundance of prevalent species in each group. Data are presented as median values with Q1 and Q3. (F) Validation of *L. murinus* abundance in *Fabp6^{fl/fl}* and *Fabp6^{ΔIEC}* mice using qRT-PCR. (G) ANI heatmap. The heatmap is generated symmetrically from OrthoANI. Statistical significance was determined using Wilcoxon test (E) and two-tailed unpaired Student's *t*-tests (F). * $p < 0.05$.

L. murinus protects *Fabp6* cKO mice from DSS-induced colitis

To evaluate the beneficial effects of *L. murinus* on DSS-induced colitis, we gavaged *Fabp6^{ΔIEC}* mice with the bacteria (1×10^9 CFU in 0.2 ml) daily for 11 days for pathophysiological analysis (34–37) or 16 days for survival analysis while administering 2.5% DSS (Fig. 5A). This intervention significantly alleviated colitis in *Fabp6^{ΔIEC}* mice, as evidenced by reduced weight loss (Fig. 5B), lower DAI score (Fig. 5C), increased colon length (Fig. 5D and E), mitigated colon tissue damage (Fig. 5F and G), and improved survival rates (Fig. 5H). Based on our observations in *Fabp6^{ΔIEC}* mice under DSS-induced colitis, we noted reduced expression of the tight junction protein Zo-1 and depletion of goblet cells, suggesting that the barrier

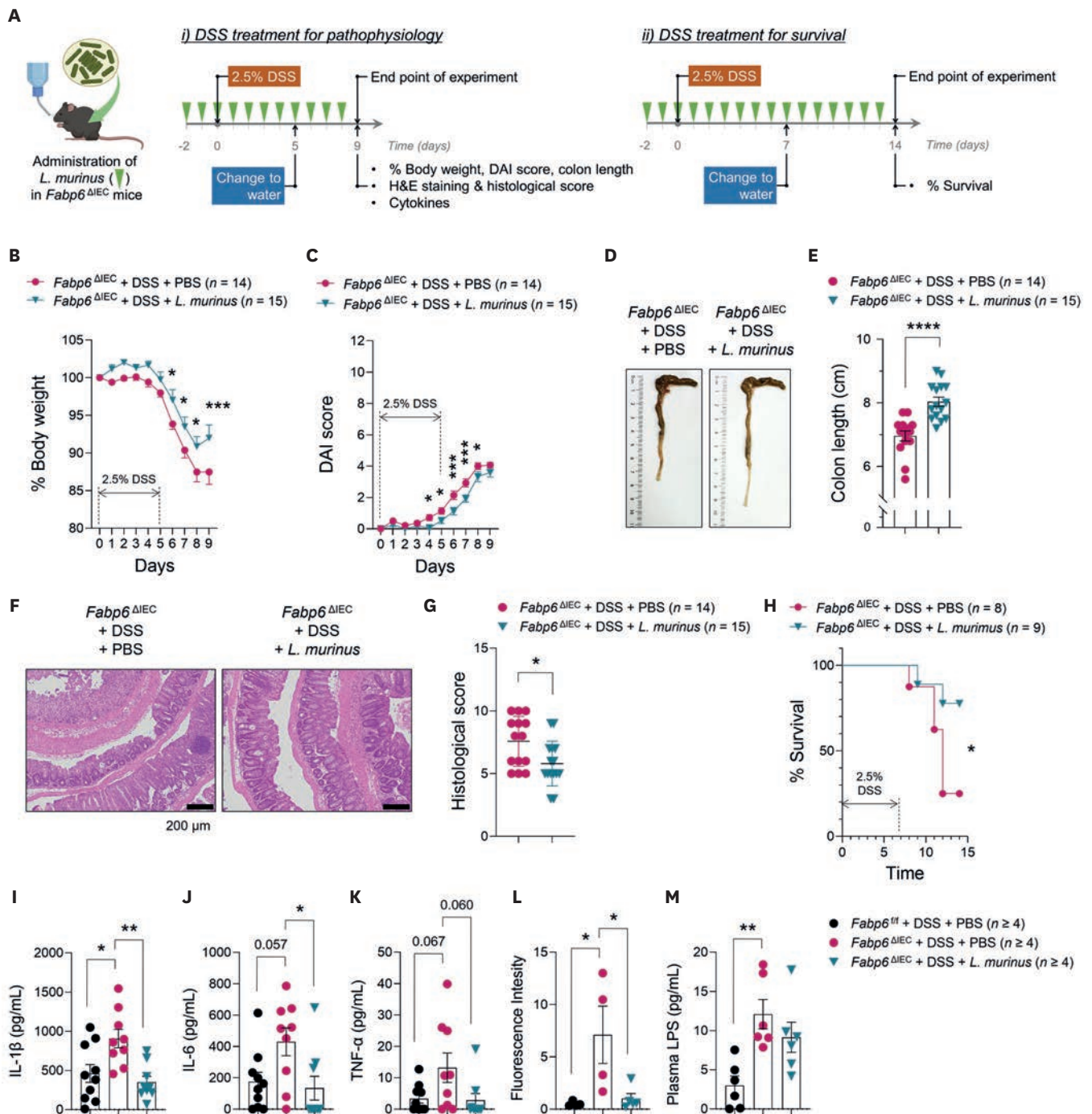


Figure 5. *Ligilactobacillus murinus* protects *Fabp6* cKO mice from DSS-mediated gut inflammation. (A) Study schemes. *Fabp6*^{ΔIEC} mice were treated daily with either PBS or *L. murinus* (1×10⁹ CFU in 0.2 ml) by oral gavage and treated with 2.5% DSS for 5 or 7 days to induce acute colitis. (B) Body weight loss and (C) DAI score were monitored daily for 9 days. Representative images of the colon (D) were taken and colon length (E) was measured on day 9. H&E staining of colon sections (F) and histological scoring (G) of PBS-treated and *L. murinus*-treated *Fabp6*^{ΔIEC} mice were performed at the end of the experiment (day 9). (H) Survival rates were monitored daily for 14 days in PBS-treated and *L. murinus*-treated *Fabp6*^{ΔIEC} mice with DSS-induced colitis (2.5% for 7 days). The levels of (I) IL-1β, (J) IL-6, and (K) TNF-α in colon tissue samples were determined by ELISA. (L) Paracellular FITC-dextran permeability was assessed in plasma samples. (M) Plasma LPS levels were determined by ELISA. A mantel cox survival analysis was used to compare the survival rates between groups. Data are presented as mean ± SEM. Statistical significance was determined using two-way ANOVA with Tukey's multiple comparisons test (B, C), two-tailed unpaired Student's *t*-tests (E, G), or one-way ANOVA with Tukey's multiple comparisons test (I–M). **p*<0.05, ***p*<0.01, ****p*<0.001, *****p*<0.0001.

integrity of *Fabp6*^{AIEC} mice was compromised by DSS treatment (**Supplementary Fig. 8A-C**). To explore the underlying mechanisms, we measured pro-inflammatory cytokine levels (IL-1 β , IL-6 and TNF- α) in the colons of three groups: DSS-treated *Fabp6*^{fl/fl} mice, DSS-treated *Fabp6*^{AIEC} mice, and *L. murinus* and DSS co-treated *Fabp6*^{AIEC} mice. DSS treatment markedly elevated the levels of IL-1 β , IL-6 and TNF- α in *Fabp6*^{AIEC} mice compared to *Fabp6*^{fl/fl} mice. Notably, *L. murinus* administration attenuated these cytokines levels in *Fabp6*^{AIEC} mice to levels comparable to those in *Fabp6*^{fl/fl} mice (**Fig. 5I-K**). Additionally, the increased paracellular FITC-dextran permeability caused by DSS was significantly ameliorated by *L. murinus* treatment (**Fig. 5L**). Although plasma LPS concentrations were elevated during colitis and reduced by *L. murinus* treatment, the reduction was not statistically significant (**Fig. 5M**). Collectively, our results demonstrate that *L. murinus* plays a crucial role in preventing DSS-induced colitis, at least in part by improving intestinal barrier function and reducing intestinal permeability.

The BAs TCA, CDCA, and TDCA, which were reduced in *Fabp6* cKO mice, promote the growth of *L. murinus*

Given the significant reductions in TCA, GCA, CA, CDCA, and TDCA levels in *Fabp6*^{AIEC} mice compared to *Fabp6*^{fl/fl} mice (**Fig. 1D**), we hypothesized that these BAs might promote the growth of *L. murinus*. To test this, we conducted an *in vitro* growth assay and found that TCA, CDCA, and TDCA—but not CA or UDCA—significantly stimulated *L. murinus* growth (**Fig. 6A-E**). Thus, the reduced levels of TCA, CDCA, and TDCA in *Fabp6*^{AIEC} mice may restrict *L. murinus* growth. Conversely, an *in vitro* growth assay with *Ligilactobacillus salivarius*, a closely related *Ligilactobacillus* spp. detected in both mouse and human feces (19), showed that only TDCA positively impacted its growth (**Fig. 6F-J**).

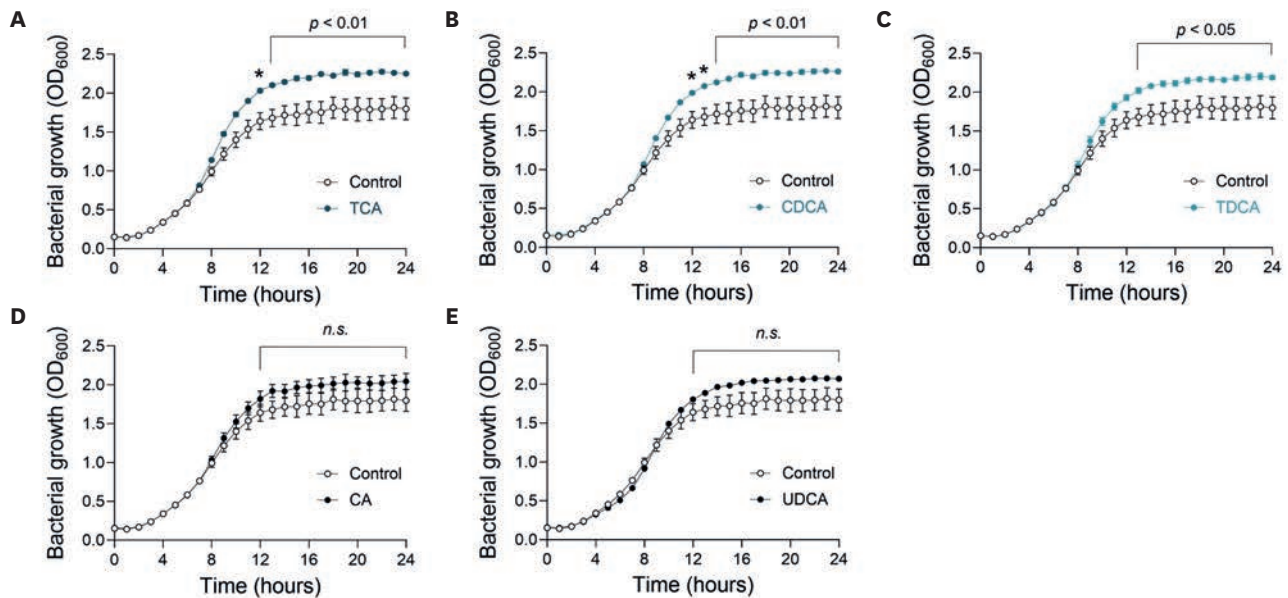
TDCA protects *Fabp6* cKO mice from DSS-induced colitis

Given that TDCA—a BA reduced in *Fabp6*^{AIEC} mice—promotes *L. murinus* growth *in vitro* (**Fig. 6C**), we examined whether TDCA supplementation could mimic the effects of *L. murinus*. Daily gavage with 10 mM TDCA, alone or combined with *L. murinus*, during DSS administration (**Fig. 7A**) resulted in similar protective effects to *L. murinus* alone: reduced weight loss (**Fig. 7B**), lower DAI (**Fig. 7C**), longer colons (**Fig. 7D and E**), and improved histopathology (**Fig. 7F and G**). TDCA also lowered colonic pro-inflammatory cytokines (**Fig. 7H-J**), decreased paracellular permeability (**Fig. 7K**), and reduced plasma LPS (**Fig. 7L**). Notably, co-administration of TDCA and *L. murinus* did not yield additive or synergistic benefits, suggesting that TDCA and *L. murinus* confer protection through a shared mechanistic pathway.

DISCUSSION

Gut microbiota profoundly influence host metabolism; however, how disruptions in host metabolic pathways reciprocally shape microbial composition remains less well understood. We hypothesized that dysregulation of BA metabolism directly disrupts the symbiotic relationship between host and gut microbiota. To test this, we deleted *Fabp6* gene specifically in IECs, which encodes a cytosolic carrier responsible for BA transport from the apical to basolateral membranes of enterocyte. Despite no significant changes in gene expression related to BA synthesis (*Cyp7a1*), transport (*Asbt* and *Osta*), homeostasis (*Fxr*, *Shp*, and *Fgf15*), or conjugation (*Bacs*) in *Fabp6*^{AIEC} mice compared to *Fabp6*^{fl/fl} mice, we observed an imbalance in BA levels in *Fabp6*^{AIEC} mice. Unlike BA homeostasis KO models such as *Fxr* (38), *Shp* (39), and *Fgf15* (40) KO mice, which exhibit elevated BA pool sizes, BA transporter

L. murinus growth assay (in vitro)



L. salivarius growth assay (in vitro)

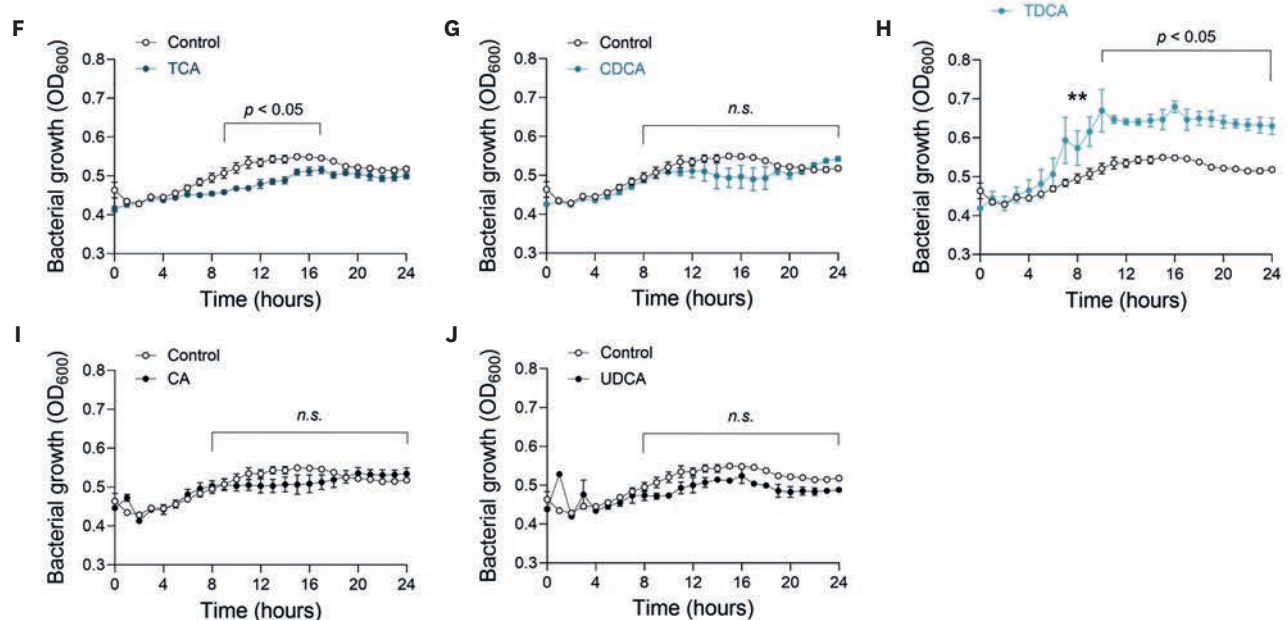


Figure 6. The reduced bile acids in *Fabp6* cKO mice promote *Ligilactobacillus* growth in vitro. (A-E) *L. murinus* was incubated with 10 μ M of TCA (A), CDCA (B), TDCA (C), CA (D), or UDCA (E) in MRS medium at 37°C for 24 h. Growth of *L. murinus* was determined by measuring the OD at 600 nm. (F-J) *L. salivarius* was incubated with 10 μ M of TCA (F), CDCA (G), TDCA (H), CA (I), or UDCA (J) in M9 minimal medium at 37°C for 24 h. Growth of *L. salivarius* was determined by measuring the OD at 600 nm. Data are presented as mean \pm SEM. Statistical significance was determined using two-way ANOVA.

n.s., not significant.

*p < 0.05, **p < 0.01.

KO models including *Asbt* (8), *Osta* (9), and *Ilbp* (10) KO mice have been reported to show reduced BA pool sizes. In the case of *Ilbp* KO mice, sex-dependent differences have also been observed in the expression of hepatic BA synthesis enzymes (e.g., *Cyp7a1*) and BA transporters (e.g., *Ntcp* and *Oatp1b2*), which may contribute to variability in BA pool size

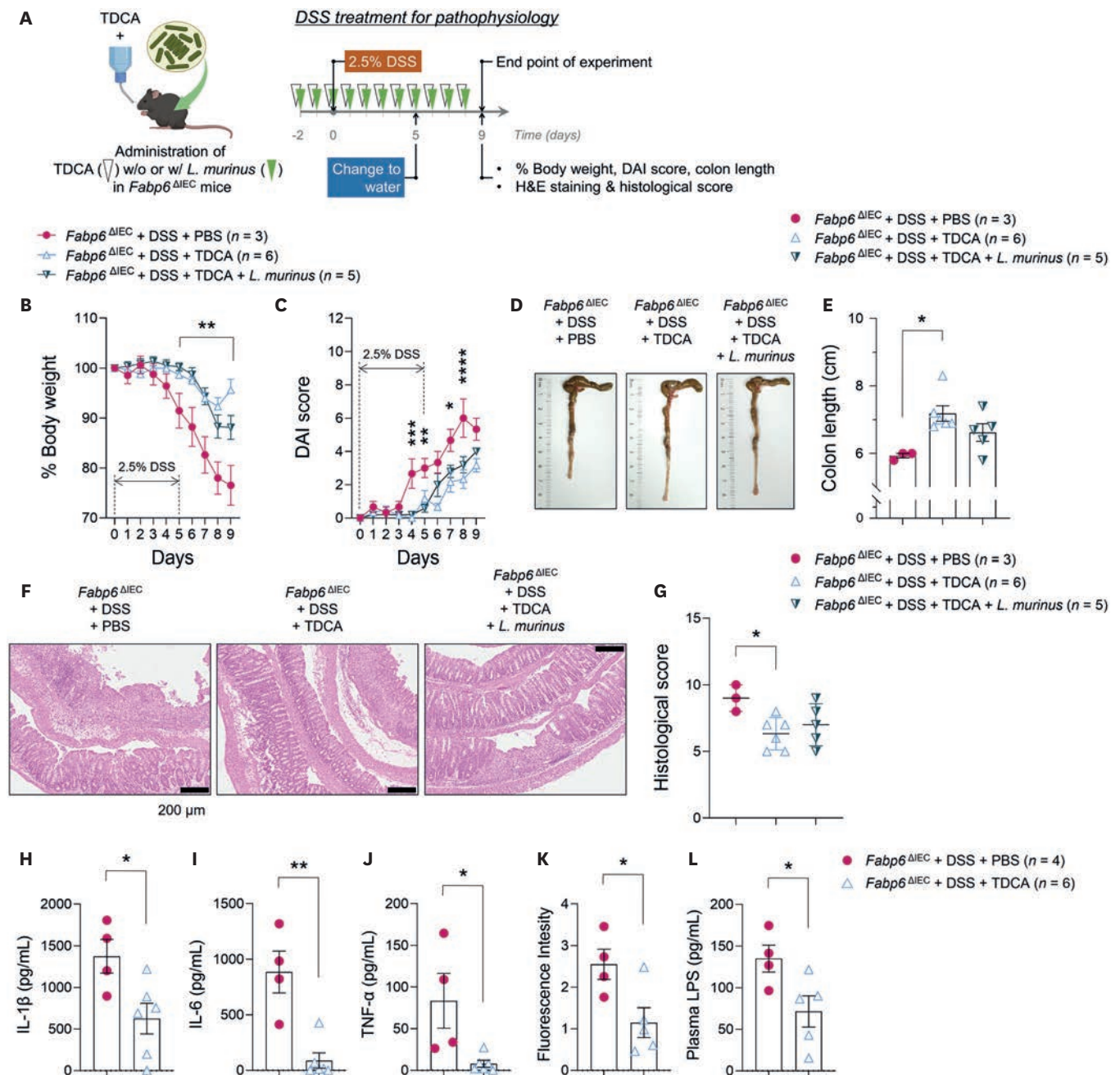


Figure 7. TDCA enhances protective effects against DSS-induced colitis. (A) Study schemes. *Fabp6^{ΔIEC}* mice were treated daily with either PBS, TDCA (10 mM), or TDCA with *L. murinus* (1×10^9 CFU in 0.2 ml) by oral gavage and treated with 2.5% DSS for 5 days to induce acute colitis. (B) Body weight loss and (C) DAI score were monitored daily for 9 days. Representative images of the colon (D) were taken and colon length (E) was measured on day 9. H&E staining of colon sections (F) and histological scoring (G) of PBS-treated, TDCA-treated, and TDCA + *L. murinus*-treated *Fabp6^{ΔIEC}* mice were performed at the end of the experiment (day 9). The levels of (H) IL-1β, (I) IL-6, and (J) TNF-α in colon tissue samples were determined by ELISA. (K) Paracellular FITC-dextran permeability was assessed in plasma samples. (L) Plasma LPS levels were determined by ELISA. Data are presented as mean \pm SEM. Statistical significance was determined using two-way ANOVA with Tukey's multiple comparisons test (B, C), one-way ANOVA with Tukey's multiple comparisons test (E, G), or two-tailed unpaired Student's *t*-tests (H-L). * $p < 0.05$, ** $p < 0.01$, *** $p < 0.001$, **** $p < 0.0001$.

and hepatic BA handling between males and females (10). Consistently, the levels of TCA, GCA, CA, CDCA, and TDCA were significantly decreased in *Fabp6^{ΔIEC}* mice compared to *Fabp6^{fl}* mice (Fig. 1D). Among these, TCA, CDCA, and TDCA promoted *L. murinus* growth in rich media (MRS), while TDCA supported *L. salivarius* growth in minimal media (M9)

(Fig. 6), indicating distinct BA utilization patterns between the 2 *Ligilactobacillus* spp. Our findings imply that specific BAs support *Ligilactobacillus* spp. growth, and that the reduced BA concentration in *Fabp6*^{ΔIEC} mice may limit *L. murinus* proliferation, though further research is needed to understand the mechanisms of BA utilization by *Ligilactobacillus* spp.

Previous work by Tang and colleagues (19) demonstrated the beneficial effect of *L. murinus* colonization on DSS-induced colitis. They showed that Dectin-1 deficiency, which affects a C-type lectin receptor, promotes *L. murinus* growth by reducing antimicrobial peptides normally induced by Dectin-1 signaling. This environment supports the development of Treg cells, thereby protecting mice from DSS-induced colitis. In contrast, in *Fabp6*^{ΔIEC} mice, where *L. murinus* levels were reduced, there was no increase in antimicrobial peptides such as S100a8, Camp, and Reg3g (Supplementary Fig. 8D-F), nor was there a change in intestinal permeability (Supplementary Fig. 1F) under normal conditions. These findings suggest that the reduced abundance of *L. murinus* in *Fabp6*^{ΔIEC} mice is due to bile acid deficiency rather than the regulation of antimicrobial peptides.

To explore the clinical relevance of *L. murinus* and gut inflammation, we analyzed metagenomic data from the Human Microbiome Project (HMP) Data Portal, which included 100 healthy individuals from HMP (41) and 100 participants with IBD from HMP2 (42). We found that the average proportion of *L. murinus* was very low (<0.01%), as was the total proportion of all *Ligilactobacillus* spp. (<0.01%) in this North American population, making difference between healthy and IBD groups statistically insignificant. However, in our analysis of healthy Korean individuals, the median proportion of all *Ligilactobacillus* spp. was higher (0.03%) (data not shown), consistent with the detection of *Ligilactobacillus* spp., specifically *L. salivarius*, in patients with CD, UC and healthy subjects in Japan (19). Although a decreased abundance of *L. salivarius* was observed in Japanese CD patients compared to healthy subjects (19), we were unable to analyze Korean IBD patients in this study due to limited access to patient samples. This discrepancy between Western and Asian populations may be attributed to variations in microbial community structure and/or ethnic or racial backgrounds.

BA plays a dual role in modulating gut microbiota. While they inhibit the growth of pathogenic bacteria such as *Clostridium difficile* (31,43), *Vibrio cholerae* (44), and vancomycin-resistant *Enterococcus* (45), they also promote the growth of commensal bacteria like *Akkermansia muciniphila* (46) and support the maturation of early-life gut microbiota, including *Lactobacillus* spp. (47). Therefore, BA-mediated microbiota modulation has significant implications for gut health. Underlying mechanisms by which BAs directly influence bacterial growth are highly specific to each case. In a precision microbiome study, researchers evaluated BA-dependent microbiota, such as *C. scindens*, and their role in inhibiting *C. difficile* infections (43). BAs mediate the crosstalk between host and microbiota through bile salt hydrolase activity, thereby inhibiting pathogens like *C. difficile* (31) and *V. cholerae* (44). Additionally, a morphotype switch in vancomycin-resistant *Enterococcus* induced by LCA highlights its potential as a non-bactericidal therapeutic approach (45). More recently, a click-chemistry-based study identified *Bacteroides uniformis*-derived 3-succinyl-CA and reported its role in alleviating metabolic-associated steatohepatitis by promoting the growth of *A. muciniphila* (46). The association between BA dysregulation and gut inflammation has been extensively studied, with most findings indicating a reduction in secondary BAs, such as DCA and LCA, in patients with IBD (42,48). In the HMP2 study, researchers found that DCA and LCA levels were reduced in the dysbiotic group of patients with CD compared

to the non-dysbiotic group (42). Similarly, a study of UC patients showed a reduction in secondary BAs in inflammation-prone UC pouches (48). Other BAs have also been reported at lower levels in IBD patient samples compared to healthy subjects. While many studies suggest an association between BA dysregulation and IBD pathogenesis, it remains unclear whether this dysregulation is a cause or a consequence of the disease. However, several mouse models with genetic modifications that disrupt BA homeostasis have demonstrated exacerbation of DSS-induced colitis (48–50). Consistent with our findings of decreased TDCA levels in *Fabp6*^{ΔIEC} mice, reduced TDCA levels have also been observed in the serum of both pediatric (51) and adult IBD patients (52). Although bacterial species possessing the *bai* operon—implicated in the reduction of secondary BAs in IBD—have been relatively well characterized (48), the specific association between *Ligilactobacillus* spp. and TDCA remains unclear. Although TDCA significantly promoted *L. murinus* growth *in vitro*, the *in vivo* intestinal environment is more complex. TDCA may be rapidly metabolized into other BA species by gut microbes, limiting its direct availability to support *L. murinus* proliferation. Moreover, the absence of an additive effect when TDCA and *L. murinus* were co-administered suggests they act within the same BA–microbiota–barrier integrity pathway. However, since we did not observe TDCA-induced *L. murinus* expansion *in vivo*, the mechanistic link remains speculative, and TDCA may also exert protective effects through *L. murinus*-independent mechanisms. Future studies using higher-resolution metagenomic sequencing, longer supplementation periods, and combined BA formulations will be necessary to determine whether BA supplementation can reliably restore *L. murinus* populations *in vivo* (53).

By analyzing barrier integrity in GF mice transplanted with fecal microbiota from either *Fabp6*^{ΔIEC} or *Fabp6*^{eff} donors, we sought to clarify whether barrier dysfunction precedes dysbiosis or vice versa. GF mice receiving *Fabp6*^{ΔIEC} microbiota exhibited elevated pro-inflammatory cytokines and plasma LPS, along with a reduction in goblet cells, compared with those receiving *Fabp6*^{eff} microbiota (**Supplementary Fig. 9**). These findings indicate that dysbiosis precedes—and likely contributes to—the onset of barrier dysfunction.

One limitation of this study is the absence of post-colonization microbiota profiling to confirm successful engraftment of donor communities and sustained depletion of *L. murinus* in GF recipient mice. Another limitation of our study is the lack of direct evidence explaining the mechanisms underlying the reduction in luminal BAs observed in *Fabp6*^{ΔIEC} mice. However, given that the levels of TCA and Tβ-MCA, which are predominantly enriched BAs in the gut of GF mice, are comparable between GF WT and GF *Fabp6*^{ΔIEC} mice (**Supplementary Fig. 10**), we propose that defective intracellular trafficking of BAs in *Fabp6*^{ΔIEC} IECs has a minor impact on BA levels. Instead, the microbiota may play a critical role in reducing luminal BA levels in *Fabp6*^{ΔIEC} mice. Further studies are needed to clarify the cause-and-effect relationship between changes in microbiota community and luminal BA concentration.

The DSS-induced colitis model is primarily characterized by epithelial barrier dysfunction, subsequently leading to an inflammatory immune response. Conversely, the *H. hepaticus*-induced colitis model is predominantly driven by immune dysregulation, with epithelial barrier function remaining relatively intact. Given these fundamental differences, it is plausible that *L. murinus* exerts distinct impacts in each colitis model. In this regard, our findings from the *H. hepaticus*-induced model suggest that the quantitative reduction of *L. murinus* in *Fabp6*^{ΔIEC} mice does not significantly alter the immune response. In contrast, we propose that *L. murinus* directly modulates epithelial barrier integrity in the DSS colitis model, thereby influencing disease severity. Supporting this hypothesis, our data indicate that *Fabp6*

deficiency in epithelial cells leads to compromised barrier integrity, as demonstrated by reduced expression of the tight junction protein Zo-1 (**Supplementary Fig. 8A**), depletion of goblet cells (**Supplementary Fig. 8B and C**), increased paracellular FITC-dextran permeability (**Figs. 5L and 7K**), and elevated plasma LPS levels (**Figs. 5M and 7L**) following DSS treatment. These alterations exacerbate susceptibility to epithelial barrier disruption and subsequent inflammation induced by DSS. However, our analyses showed no significant impact of *Fabp6* deficiency on the expression of genes associated with antimicrobial peptides (**Supplementary Fig. 8D-F**) or bile acid homeostasis (**Supplementary Fig. 2B-K**) under colitis, both critical for maintaining barrier function.

L. murinus may strengthen epithelial barrier integrity by enhancing tight junction protein expression and promoting goblet cell functions, such as mucus production and secretion. This improved barrier integrity would consequently reduce the translocation of luminal Ags and bacteria, which are major drivers of inflammation in colitis models (54,55). To investigate potential immune-regulatory mechanisms more deeply, we conducted additional experiments aimed at identifying specific immune cell populations regulated by *L. murinus*. Through flow cytometry analyses, we evaluated changes in multiple intestinal immune cell types—including Tregs, Th1 and Th17 cells, macrophages, dendritic cells, and granulocytes—in DSS-treated *Fabp6*^{ΔIEC} mice supplemented with or without *L. murinus* (**Supplementary Fig. 11A-I**). Our results indicate that the majority of these immune cell populations were not significantly altered by *L. murinus* supplementation. Notably, however, the number of recently recruited inflammatory monocytes (Ly6C⁺MHCII⁺ monocytes), which significantly increased in *Fabp6*^{ΔIEC} mice during DSS-induced colitis, was restored to control levels following *L. murinus* supplementation (**Supplementary Fig. 11G**). This suggests that *L. murinus* effectively reduces monocyte infiltration into damaged intestinal tissues. Taken together, our findings support a mechanism wherein *L. murinus* exerts its protective effect primarily through enhancement of epithelial barrier integrity rather than by direct modulation of intestinal immune cell populations. Additionally, while previous studies indicate that certain *Lactobacillus* spp. can modulate immune responses by shifting T-cell differentiation toward regulatory phenotypes (19), our current results did not detect significant changes in intestinal T-cell populations following *L. murinus* supplementation.

In summary, we demonstrated that the *Fabp6* deletion triggers an imbalance in BA and dysbiosis, with a significant reduction in the abundance of *L. murinus*. Colonization of *L. murinus* or supplementation of TDCA in *Fabp6*^{ΔIEC} mice alleviates DSS-induced colitis by improving epithelial barrier integrity and reducing pro-inflammatory cytokines (**Supplementary Fig. 12**). These findings highlight the critical role of symbiotic interactions between intestinal microbiota and host metabolism in regulating gut inflammation.

ACKNOWLEDGEMENTS

This work was supported by the National Research Foundation of Korea (NRF) grants funded by the Korea government (MSIT) (2022M3A9F3017506, 2022M3A9F3094557, and RS-2024-00340699 to J.-H.R.; RS-2023-00250400 to Y.W.C.), and by a grant of the MD-PhD/Medical Scientist Training Program through the Korea Health Industry Development Institute (KHIDI), funded by the Ministry of Health & Welfare, Republic of Korea (B0080327004045 to Y.J.).

SUPPLEMENTARY MATERIALS

Supplementary Data 1

Materials and methods

Supplementary Table 1

Schematic overview of primary, conjugated, and secondary BA species

Supplementary Table 2

Primers used for RT-qPCR

Supplementary Table 3

GCF numbers for *Ligilactobacillus* and *Ligilactobacillus murinus* genomes

Supplementary Figure 1

Comparison of bile acid metabolism-related gene expression between WT and *Fabp6* cKO mice.

Supplementary Figure 2

Comparison of bile acid metabolism-related gene expression between WT and *Fabp6* cKO mice under normal conditions and DSS-induced colitis.

Supplementary Figure 3

Immune cell profile analysis of *H. hepaticus*-induced colitis model.

Supplementary Figure 4

Flow cytometry analysis of T cells in the ileum, colon, and mesenteric lymph nodes (mLN) of WT and *Fabp6* cKO mice.

Supplementary Figure 5

Flow cytometry analysis of myeloid cells in the ileum, colon, and mLN of WT and *Fabp6* cKO mice.

Supplementary Figure 6

Relative abundance of pathway categories based on KEGG databases.

Supplementary Figure 7

Comparative genomic analysis with dispensable genes of *Ligilactobacillus* species.

Supplementary Figure 8

Comparison of tight junction protein Zo-1, goblet cells, and antimicrobial peptides between WT and *Fabp6* cKO mice under normal conditions and DSS-induced colitis.

Supplementary Figure 9

Comparison of pro-inflammatory cytokines, LPS, and goblet cells in GF FMT mice under normal conditions and DSS-induced colitis.

Supplementary Figure 10

Comparison of metabolites between SPF and GF *Fabp6* cKO mice.

Supplementary Figure 11

Monocyte infiltration is accompanied by increased severity of DSS-induced colitis in *Fabp6* cKO mice.

Supplementary Figure 12

Proposed model of the protective effect of *L. murinus* and TDCA in DSS-induced gut inflammation.

REFERENCES

1. Russell DW. The enzymes, regulation, and genetics of bile acid synthesis. *Annu Rev Biochem* 2003;72:137-174. [PUBMED](#) | [CROSSREF](#)
2. Boyer JL. Bile formation and secretion. *Compr Physiol* 2013;3:1035-1078. [PUBMED](#) | [CROSSREF](#)
3. de Aguiar Vallim TQ, Tarling EJ, Edwards PA. Pleiotropic roles of bile acids in metabolism. *Cell Metab* 2013;17:657-669. [PUBMED](#) | [CROSSREF](#)
4. Oelkers P, Kirby LC, Heubi JE, Dawson PA. Primary bile acid malabsorption caused by mutations in the ileal sodium-dependent bile acid transporter gene (SLC10A2). *J Clin Invest* 1997;99:1880-1887. [PUBMED](#) | [CROSSREF](#)
5. Makishima M, Okamoto AY, Repa JJ, Tu H, Learned RM, Luk A, Hull MV, Lustig KD, Mangelsdorf DJ, Shan B. Identification of a nuclear receptor for bile acids. *Science* 1999;284:1362-1365. [PUBMED](#) | [CROSSREF](#)
6. Dawson PA, Hubbert M, Haywood J, Craddock AL, Zerangue N, Christian WV, Ballatori N. The heteromeric organic solute transporter α - β , Osta-Ost β , is an ileal basolateral bile acid transporter. *J Biol Chem* 2005;280:6960-6968. [PUBMED](#) | [CROSSREF](#)
7. Inagaki T, Choi M, Moschetta A, Peng L, Cummins CL, McDonald JG, Luo G, Jones SA, Goodwin B, Richardson JA, et al. Fibroblast growth factor 15 functions as an enterohepatic signal to regulate bile acid homeostasis. *Cell Metab* 2005;2:217-225. [PUBMED](#) | [CROSSREF](#)
8. Dawson PA, Haywood J, Craddock AL, Wilson M, Tietjen M, Kluckman K, Maeda N, Parks JS. Targeted deletion of the ileal bile acid transporter eliminates enterohepatic cycling of bile acids in mice. *J Biol Chem* 2003;278:33920-33927. [PUBMED](#) | [CROSSREF](#)
9. Rao A, Haywood J, Craddock AL, Belinsky MG, Kruh GD, Dawson PA. The organic solute transporter α - β , Osta-Ost β , is essential for intestinal bile acid transport and homeostasis. *Proc Natl Acad Sci U S A* 2008;105:3891-3896. [PUBMED](#) | [CROSSREF](#)
10. Praslickova D, Torchia EC, Sugiyama MG, Magrane EJ, Zwicker BL, Kolodzieyski L, Agellon LB. The ileal lipid binding protein is required for efficient absorption and transport of bile acids in the distal portion of the murine small intestine. *PLoS One* 2012;7:e50810. [PUBMED](#) | [CROSSREF](#)
11. Habib SM, Zwicker BL, Wykes L, Agellon LB. Sexually dimorphic response of mice to the Western-style diet caused by deficiency of fatty acid binding protein 6 (*Fabp6*). *Physiol Rep* 2021;9:e14733. [PUBMED](#) | [CROSSREF](#)
12. Kostic AD, Xavier RJ, Gevers D. The microbiome in inflammatory bowel disease: current status and the future ahead. *Gastroenterology* 2014;146:1489-1499. [PUBMED](#) | [CROSSREF](#)
13. Lynch SV, Pedersen O. The human intestinal microbiome in health and disease. *N Engl J Med* 2016;375:2369-2379. [PUBMED](#) | [CROSSREF](#)
14. Hooper LV, Wong MH, Thelin A, Hansson L, Falk PG, Gordon JI. Molecular analysis of commensal host-microbial relationships in the intestine. *Science* 2001;291:881-884. [PUBMED](#) | [CROSSREF](#)
15. Ananthakrishnan AN. Epidemiology and risk factors for IBD. *Nat Rev Gastroenterol Hepatol* 2015;12:205-217. [PUBMED](#) | [CROSSREF](#)
16. Frank DN, St Amand AL, Feldman RA, Boedeker EC, Harpaz N, Pace NR. Molecular-phylogenetic characterization of microbial community imbalances in human inflammatory bowel diseases. *Proc Natl Acad Sci U S A* 2007;104:13780-13785. [PUBMED](#) | [CROSSREF](#)
17. Neurath MF. Cytokines in inflammatory bowel disease. *Nat Rev Immunol* 2014;14:329-342. [PUBMED](#) | [CROSSREF](#)
18. Steidler L, Hans W, Schotte L, Neirynck S, Obermeier F, Falk W, Fiers W, Remaut E. Treatment of murine colitis by *Lactococcus lactis* secreting interleukin-10. *Science* 2000;289:1352-1355. [PUBMED](#) | [CROSSREF](#)

19. Tang C, Kamiya T, Liu Y, Kadoki M, Kakuta S, Oshima K, Hattori M, Takeshita K, Kanai T, Saijo S, et al. Inhibition of dectin-1 signaling ameliorates colitis by inducing *Lactobacillus*-mediated regulatory T cell expansion in the intestine. *Cell Host Microbe* 2015;18:183-197. [PUBMED](#) | [CROSSREF](#)
20. Strober W, Fuss I, Mannon P. The fundamental basis of inflammatory bowel disease. *J Clin Invest* 2007;117:514-521. [PUBMED](#) | [CROSSREF](#)
21. Gevers D, Kugathasan S, Denson LA, Vázquez-Baeza Y, Van Treuren W, Ren B, Schwager E, Knights D, Song SJ, Yassour M, et al. The treatment-naïve microbiome in new-onset Crohn's disease. *Cell Host Microbe* 2014;15:382-392. [PUBMED](#) | [CROSSREF](#)
22. Khor B, Gardet A, Xavier RJ. Genetics and pathogenesis of inflammatory bowel disease. *Nature* 2011;474:307-317. [PUBMED](#) | [CROSSREF](#)
23. Chung YW, Cha J, Han S, Chen Y, Gucek M, Cho HJ, Nakahira K, Choi AMK, Ryu JH, Yoon JH. Apolipoprotein E and periostin are potential biomarkers of nasal mucosal inflammation. A parallel approach of *in vitro* and *in vivo* secretomes. *Am J Respir Cell Mol Biol* 2020;62:23-34. [PUBMED](#) | [CROSSREF](#)
24. Erben U, Loddenkemper C, Doerfel K, Spieckermann S, Haller D, Heimesaat MM, Zeitz M, Siegmund B, Kühl AA. A guide to histomorphological evaluation of intestinal inflammation in mouse models. *Int J Clin Exp Pathol* 2014;7:4557-4576. [PUBMED](#)
25. Wood DE, Salzberg SL. Kraken: ultrafast metagenomic sequence classification using exact alignments. *Genome Biol* 2014;15:R46. [PUBMED](#) | [CROSSREF](#)
26. Lu J, Breitwieser FP, Thielen P, Salzberg SL. Bracken: estimating species abundance in metagenomics data. *PeerJ Comput Sci* 2017;3:e104. [PUBMED](#) | [CROSSREF](#)
27. Morris EK, Caruso T, Buscot F, Fischer M, Hancock C, Maier TS, Meiners T, Müller C, Obermaier E, Prati D, et al. Choosing and using diversity indices: insights for ecological applications from the German Biodiversity Exploratories. *Ecol Evol* 2014;4:3514-3524. [PUBMED](#) | [CROSSREF](#)
28. Kanehisa M, Goto S. KEGG: Kyoto Encyclopedia of Genes and Genomes. *Nucleic Acids Res* 2000;28:27-30. [PUBMED](#) | [CROSSREF](#)
29. Buchfink B, Xie C, Huson DH. Fast and sensitive protein alignment using DIAMOND. *Nat Methods* 2015;12:59-60. [PUBMED](#) | [CROSSREF](#)
30. Song X, Sun X, Oh SF, Wu M, Zhang Y, Zheng W, Geva-Zatorsky N, Jupp R, Mathis D, Benoist C, et al. Microbial bile acid metabolites modulate gut ROR γ ⁺ regulatory T cell homeostasis. *Nature* 2020;577:410-415. [PUBMED](#) | [CROSSREF](#)
31. Foley MH, Walker ME, Stewart AK, O'Flaherty S, Gentry EC, Patel S, Beaty VV, Allen G, Pan M, Simpson JB, et al. Bile salt hydrolases shape the bile acid landscape and restrict *Clostridioides difficile* growth in the murine gut. *Nat Microbiol* 2023;8:611-628. [PUBMED](#) | [CROSSREF](#)
32. Storch J, Corsico B. The multifunctional family of mammalian fatty acid-binding proteins. *Annu Rev Nutr* 2023;43:25-54. [PUBMED](#) | [CROSSREF](#)
33. Xu M, Pokrovskii M, Ding Y, Yi R, Au C, Harrison OJ, Galan C, Belkaid Y, Bonneau R, Littman DR. c-MAF-dependent regulatory T cells mediate immunological tolerance to a gut pathobiont. *Nature* 2018;554:373-377. [PUBMED](#) | [CROSSREF](#)
34. Brown DG, Murphy M, Cadeddu R, Bell R, Weis A, Chiaro T, Klag K, Morgan J, Coon H, Stephens WZ, et al. Colitis reduces active social engagement in mice and is ameliorated by supplementation with human microbiota members. *Nat Commun* 2024;15:2769. [PUBMED](#) | [CROSSREF](#)
35. Gaifem J, Mendes-Frias A, Wolter M, Steimle A, Garzón MJ, Ubeda C, Nobre C, González A, Pinho SS, Cunha C, et al. *Akkermansia muciniphila* and *Parabacteroides distasonis* synergistically protect from colitis by promoting ILC3 in the gut. *MBio* 2024;15:e0007824. [PUBMED](#) | [CROSSREF](#)
36. Huang J, Yang Z, Li Y, Chai X, Liang Y, Lin B, Ye Z, Zhang S, Che Z, Zhang H, et al. *Lactobacillus paracasei* R3 protects against dextran sulfate sodium (DSS)-induced colitis in mice via regulating Th17/Treg cell balance. *J Transl Med* 2021;19:356. [PUBMED](#) | [CROSSREF](#)
37. Li Q, Sun X, Yu K, Lv J, Miao C, Yang J, Wang S, Fu Z, Sun Y, Zhang H, et al. *Enterobacter ludwigii* protects DSS-induced colitis through choline-mediated immune tolerance. *Cell Reports* 2022;40:111308. [PUBMED](#) | [CROSSREF](#)
38. Kok T, Hulzebos CV, Wolters H, Havinga R, Agellon LB, Stellaard F, Shan B, Schwarz M, Kuipers F. Enterohepatic circulation of bile salts in farnesoid X receptor-deficient mice: efficient intestinal bile salt absorption in the absence of ileal bile acid-binding protein. *J Biol Chem* 2003;278:41930-41937. [PUBMED](#) | [CROSSREF](#)
39. Shaw RPH, Kolyvas P, Dang N, Hyon A, Bailey K, Anakk S. Loss of hepatic small heterodimer partner elevates ileal bile acids and alters cell cycle-related genes in male mice. *Endocrinology* 2022;163:bqac052. [PUBMED](#) | [CROSSREF](#)

40. Bozadjieva-Kramer N, Shin JH, Shao Y, Gutierrez-Aguilar R, Li Z, Heppner KM, Chiang S, Vargo SG, Granger K, Sandoval DA, et al. Intestinal-derived FGF15 protects against deleterious effects of vertical sleeve gastrectomy in mice. *Nat Commun* 2021;12:4768. [PUBMED](#) | [CROSSREF](#)
41. Human Microbiome Project Consortium. Structure, function and diversity of the healthy human microbiome. *Nature* 2012;486:207-214. [PUBMED](#) | [CROSSREF](#)
42. Lloyd-Price J, Arze C, Ananthakrishnan AN, Schirmer M, Avila-Pacheco J, Poon TW, Andrews E, Ajami NJ, Bonham KS, Brislawn CJ, et al.; IBDMDB Investigators. Multi-omics of the gut microbial ecosystem in inflammatory bowel diseases. *Nature* 2019;569:655-662. [PUBMED](#) | [CROSSREF](#)
43. Buffie CG, Bucci V, Stein RR, McKenney PT, Ling L, Gobourne A, No D, Liu H, Kinnebrew M, Viale A, et al. Precision microbiome reconstitution restores bile acid mediated resistance to *Clostridium difficile*. *Nature* 2015;517:205-208. [PUBMED](#) | [CROSSREF](#)
44. Alavi S, Mitchell JD, Cho JY, Liu R, Macbeth JC, Hsiao A. Interpersonal gut microbiome variation drives susceptibility and resistance to cholera infection. *Cell* 2020;181:1533-1546.e13. [PUBMED](#) | [CROSSREF](#)
45. McKenney PT, Yan J, Vaubourgeix J, Becattini S, Lampen N, Motzer A, Larson PJ, Dannaoui D, Fujisawa S, Xavier JB, et al. Intestinal bile acids induce a morphotype switch in vancomycin-resistant enterococcus that facilitates intestinal colonization. *Cell Host Microbe* 2019;25:695-705.e5. [PUBMED](#) | [CROSSREF](#)
46. Nie Q, Luo X, Wang K, Ding Y, Jia S, Zhao Q, Li M, Zhang J, Zhuo Y, Lin J, et al. Gut symbionts alleviate MASH through a secondary bile acid biosynthetic pathway. *Cell* 2024;187:2717-2734.e33. [PUBMED](#) | [CROSSREF](#)
47. van Best N, Rolle-Kampczyk U, Schaap FG, Basic M, Olde Damink SWM, Bleich A, Savelkoul PHM, von Bergen M, Penders J, Hornef MW. Bile acids drive the newborn's gut microbiota maturation. *Nat Commun* 2020;11:3692. [PUBMED](#) | [CROSSREF](#)
48. Sinha SR, Haileselassie Y, Nguyen LP, Tropini C, Wang M, Becker LS, Sim D, Jarr K, Spear ET, Singh G, et al. Dysbiosis-induced secondary bile acid deficiency promotes intestinal inflammation. *Cell Host Microbe* 2020;27:659-670.e5. [PUBMED](#) | [CROSSREF](#)
49. Gadaleta RM, van Erpecum KJ, Oldenburg B, Willemsen EC, Renooij W, Murzilli S, Klomp LW, Siersema PD, Schipper ME, Danese S, et al. Farnesoid X receptor activation inhibits inflammation and preserves the intestinal barrier in inflammatory bowel disease. *Gut* 2011;60:463-472. [PUBMED](#) | [CROSSREF](#)
50. Bozadjieva-Kramer N, Shin JH, Li Z, Rupp AC, Miller N, Kernodle S, Lanthier N, Henry P, Seshadri N, Myronovych A, et al. Intestinal FGF15 regulates bile acid and cholesterol metabolism but not glucose and energy balance. *JCI Insight* 2024;9:e174164. [PUBMED](#) | [CROSSREF](#)
51. Chen W, Wang D, Deng X, Zhang H, Dong D, Su T, Lu Q, Jiang C, Ni Q, Cui Y, et al. Bile acid profiling as an effective biomarker for staging in pediatric inflammatory bowel disease. *Gut Microbes* 2024;16:2323231. [PUBMED](#) | [CROSSREF](#)
52. Xu RH, Shen JN, Lu JB, Liu YJ, Song Y, Cao Y, Wang ZH, Zhang J. Bile acid profiles and classification model accuracy for inflammatory bowel disease diagnosis. *Medicine (Baltimore)* 2024;103:e38457. [PUBMED](#) | [CROSSREF](#)
53. Zou Y, Ghaderpour A, Munkhbileg B, Seo SU, Seong SY. Taurodeoxycholate ameliorates DSS-induced colitis in mice. *Int Immunopharmacol* 2023;122:110628. [PUBMED](#) | [CROSSREF](#)
54. Mukohda M, Yano T, Matsui T, Nakamura S, Miyamae J, Toyama K, Mitsui R, Mizuno R, Ozaki H. Treatment with *Ligilactobacillus murinus* lowers blood pressure and intestinal permeability in spontaneously hypertensive rats. *Sci Rep* 2023;13:15197. [PUBMED](#) | [CROSSREF](#)
55. Pan F, Zhang L, Li M, Hu Y, Zeng B, Yuan H, Zhao L, Zhang C. Predominant gut *Lactobacillus murinus* strain mediates anti-inflammation effects in calorie-restricted mice. *Microbiome* 2018;6:54. [PUBMED](#) | [CROSSREF](#)